Machine learning-based noise diagnostics for water-cooled SMRs: proof of principle on 2-dimensional systems

Progress in Nuclear Energy 189 (2025) 105950

Contents lists available at ScienceDirect

Progress in Nuclear Energy

journal homepage: www.elsevier.com/locate/pnucene

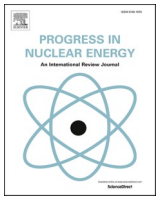

Machine learning-based noise diagnostics for water-cooled SMRs: proof of principle on 2-dimensional systems

Salma Magdi Hussein [a,b,*], Christophe Demazière [a]

[a] Department of Physics, Chalmers University of Technology, Gothenburg, SE-41296, Sweden
[b] Nuclear and Radiation Engineering Department, Faculty of Engineering, Alexandria University, Egypt

ARTICLE INFO

Keywords:
Neutron noise
SMR
Machine learning
Core monitoring
Core diagnostics

ABSTRACT

This study explores a core monitoring approach for two-dimensional Small Modular Reactors (SMRs) using neutron noise analysis and machine learning (ML) methods. Absorber of Variable Strength (AVS) perturbations are simulated in the frequency domain to analyze reactor noise behavior differences between large reactors and SMRs. It is demonstrated that SMRs exhibit stronger point-kinetic characteristics, complicating perturbation diagnosis. Thermal-group neutron noise is found to carry more diagnostic information than fast-group neutron noise. This makes thermal-group neutron noise more effective for localizing perturbations. A convolutional neural network (CNN) is trained on a dataset that contains only one or two AVS sources per sample. Despite this limited training dataset, the model can accurately localize up to 10 sources in a sample. The results demonstrate the model's strong generalization capability and high nodal accuracy. To address sparse detector scenarios, a two-stage pipeline is designed to reconstruct full reactor noise fields from limited data points prior to source localization. The pipeline demonstrates effective reconstruction and localization with 50 % detector coverage, accurately capturing both global and local noise components. For reduced instrumentation scenarios of 11 %, 6 %, and 3 % coverage, the model retains reasonable performance, with proximity-based metrics indicating robust localization capabilities. The results highlight the importance of strategic detector placement to balance global and local noise components for effective anomaly detection. The research demonstrates that ML techniques can enhance neutron noise analysis, even under limited data availability. This work contributes to enhancing the safety and operational reliability of SMRs, emphasizing the importance of advanced monitoring methods and data-informed instrumentation layouts to optimize performance, safety, and efficiency.

1. Introduction

Small Modular Reactors (SMRs) are gaining interest worldwide as a potential solution for clean energy in the future due to their compact design, availability, and enhanced safety features (IAEA, 2022a). Unlike conventional large reactors, SMRs are designed with smaller cores and operate at reduced power levels, which facilitates compliance with safety requirements. SMRs also have reduced capital investments and better availability due to modular and standardized components (Hussein, 2020). A new technology such as SMR requires the development of methods for monitoring its behavior to ensure its safety and reliable operation. These methods are essential for the early detection of anomalies within the reactor core, enabling intervention before they escalate into severe issues that could compromise reactor safety. Due to the difference in properties between SMRs and conventional reactors, methods should be studied for SMR conditions and geometries.

A promising approach for the early identification of perturbations within the reactor core is the analysis of reactor neutron noise (Pázsit and Demazière, 2010). In a nuclear reactor, the measured neutron flux contains fluctuations around the mean value, even at steady-state conditions. These fluctuations are called neutron noise, and they arise from the stochastic properties of nuclear reactions and possible perturbations of the medium in which such reactions take place. Neutron noise can be defined as the small stationary fluctuations found when measuring the neutron flux. They contain valuable information about underlying disturbances in the reactor core. By analyzing these fluctuations, operators can detect anomalies such as structural vibrations, temperature and density variations, coolant flow perturbations, or changes in core compositions, ensuring the safe and efficient operation of the reactor. Analysis of the signal noise offers a wide range of applications such as

* Corresponding author. Department of Physics, Chalmers University of Technology, Gothenburg, SE-41296, Sweden
E-mail addresses: salma.hussein@chalmers.se, salma.magdi@alexu.edu.eg (S.M. Hussein).

https://doi.org/10.1016/j.pnucene.2025.105950
Received 5 February 2025; Received in revised form 30 June 2025; Accepted 21 July 2025
Available online 28 July 2025

perturbation diagnosis, estimation of dynamic core parameters, and detection of turbulence and mechanical vibrations (IAEA, 2013).

The study of neutron noise dates back to the 1940s, with initial findings being documented during that period (De Hoffman, 1946). It was found that information from neutron noise can be used to derive power reactor transfer function (Moore, 1958) which can be used to understand the feedback effects of different phenomena inside the reactor on the neutron flux (Rajagopal, 1962). This has been studied by neutron noise pioneers, where the system variables such as the reactor power and the delayed neutron fraction were obtained from reactor noise information. In addition, oscillator experiments were carried out with different frequencies, where a spatial local component was found in the region of the applied oscillation. The local component had a higher neutron noise amplitude than the global component which is spread throughout the system (Weinberg and Schweinler, 1948). Other studies were done to study the effect of motion phenomena on the neutron noise such as the movement of control rods and the vibration of different structural components (Thie, 1963). Neutron noise for reactor diagnostics involves the construction of a model describing the noise source in the system and calculating the induced neutron noise using the system's transfer function. Thus, since early days, researchers were developing foundational models that describe how perturbations behave in different types of power reactors and how they impact the neutron noise (Thie, 1981; Williams, 1974).

Neutron noise analysis has been widely studied in commercial large-scale reactors, with emphasis on theoretical and modelling developments as well as experimental validation of these approaches (Hursin et al., 2023). Further studies addressed point-kinetic behavior on one hand and global and local noise components on the other hand (Analytis, 1979). Studies on perturbation types, such as vibrating fuel assemblies, vibrating control rods, propagating coolant disturbances, and absorbers of variable strength (AVS) emphasized the importance of the deviation from point-kinetic component of neutron noise in identifying perturbation characteristics and locations. However, most of these studies were conducted on conventional reactor systems, and only a few were concerned with comparing the neutron noise behavior in large and small systems (Demazière et al., 2022; Hussein et al., 2024). The small core size in SMRs enhances the dominance of point kinetic noise, making it difficult to isolate and analyze local noise contributions. In this paper, we will discuss the unique challenges in reactor noise analysis due to the effect of reduced size in SMRs. Hence, we will also develop a neutron noise localization technique suitable for these small systems.

This paper focuses on neutron noise behavior in SMRs, particularly in the context of anomaly detection and localization. Due to the complex nature of neutron noise and the sparsity of information acquired by neutron detectors, advanced methods such as Machine Learning (ML) are required to extract relevant information.

Studies applying Machine learning (ML) and Artificial Intelligence (AI) have shown advancements in various fields including nuclear and radiation detection fields. There is ongoing work in nuclear applications such as medical imaging, radiotherapy, and nuclear nutrition assessment. In nuclear fusion, AI studies have shown potential in different areas such as creating surrogate models and developing hybrid models that combine data-driven and physics-based approaches. In the nuclear power industry, AI studies demonstrated its applicability in various aspects, such as in automation, which can reduce safety risks in critical situations. It also showed potential in optimization of reactor design, which can increase the efficiency of the nuclear power plant. In radiation protection and nuclear security, research using AI showed promise in improving the detection and accounting of nuclear materials and control systems. In nuclear safeguards, AI holds significant opportunities to improve safeguards processes by classifying data and accounting for missing fissile material. Machine learning can also be used in predicting events inside the nuclear reactor such as potential failures, presence of anomalies, and in evaluating the current state of components. Data used for these predictions mainly comes from detectors and sensors placed in the reactor to monitor its state. Analyzing neutron noise signals using ML has a great potential since neutron noise is measured online with no disturbance to the reactor operation and ML provides a fast analysis method. Despite the numerous applications where ML demonstrate significant promise in nuclear power, its application requires thorough validation and adherence to regulatory processes, which it does not yet fully satisfy (IAEA, 2022b).

Neutron noise numerical techniques, such as Green's function inversion, provide an exact solution for perturbation identification problems. However, this requires the knowledge of the spatial neutron flux distribution everywhere inside the nuclear core. In practical reactor environments, the spatial distribution of neutron detectors is typically sparse, often limited to ex-core and a small number of in-core measurements. Thus, the sparse neutron noise information requires more advanced techniques to extract meaningful information. In this case, ML methods provide a solution, since they are well-suited to infer complex mappings from limited and noisy data without the need for explicit inversion or idealized assumptions.

Given this potential, advancements in deep learning have been applied to neutron noise analysis and for anomaly detection in different works. A study used the time series of delayed neutron count for anomaly detection by applying a nearest-neighbor-based technique. The approach aimed to detect potential anomalies indicative of leaks in nuclear reactor channels, supporting predictive maintenance in nuclear power plants (Agarwal et al., 2013). Other studies investigated the use of machine learning techniques in hexagonal reactors. Some studies aimed to reconstruct the noise sources using ANNs (Hosseini and Vosoughi, 2014), while others aimed to identify and localize perturbed fuel assemblies using decision tree, random forest, k-nearest neighbors, multilayer perceptron, support vector machine, and 1D-convolutional neural network (Kamkar and Abbasi, 2025). A separate research proposed an anomaly detection framework using neutron noise in the time domain by applying Recurrent Neural Networks (RNN) and in the frequency domain using 3D convolutional neural networks (Durrant et al., 2019).

Advanced ML methods were studied for typical large reactors showing significant potential in diagnosing and identifying different perturbations in the core (Kollias et al., 2022). This was studied within the CORTEX project which launched in 2017 seeking to advance neutron noise-based core monitoring techniques for early anomaly detection in nuclear power plants. Running for four years, it addressed the complexities of interpreting neutron noise by employing ML algorithms trained on simulated data. The project prioritized the development of mechanical and neutronic models to simulate neutron noise, which were verified computationally and validated experimentally. Additionally, different methods were employed to optimize ML architectures for precise anomaly detection and characterization (Demazière, 2025).

In this work, we make use of advances in machine learning by presenting a methodology that combines physics-based noise modeling observations with data-driven techniques to localize noise sources in SMRs, even under challenging conditions such as limited instrumentation. The study explores the theoretical basis of neutron noise, introduces novel methods for handling complex noise data using machine learning, and evaluates the performance of these methods under practical constraints.

The structure of this paper is organized as follows: Section 2 describes the SMR system employed in this study along with details of the perturbation type considered. Section 3 discusses physics-based considerations for neutron noise in SMRs, highlighting the key differences between conventional large reactors and smaller reactors. In Section 4, the application of ML is shown for detecting perturbation locations from full-core reactor noise. The datasets and model development are presented, followed by a detailed analysis of the results. Section 5 addresses the problem of instrumentation availability in the reactor, aiming at reconstructing the neutron noise from sparse detectors before proceeding with perturbation localization. Finally, Section 6 concludes the

paper by summarizing the key findings, discussing their implications for SMR design, and outlining potential directions for future research.

2. Description of the system studied

2.1. Small modular reactor model

For this study, a critical SMR core is derived from a typical large Pressurized Water Reactor (PWR). We consider a 2-dimensional (2D) plane of an SMR with an equivalent diameter of 172 cm and an active fuel region of 150.5 cm. The 2D SMR has 37 assemblies surrounded by a reflector as shown in Fig. 1. The reactor core is modelled using CORE SIM+, a two-energy group, diffusion-based neutron noise solver in the frequency domain (Mylonakis et al., 2021). CORE SIM + calculates the static flux, adjoint flux, and reactor noise in the fast and thermal neutron energy groups. The code calculates the first-order neutron noise assuming small stationary perturbations in the cross-sections at a certain frequency, according to the following equation:

$$\left\{\nabla.[\boldsymbol{D}(\boldsymbol{r})\nabla] + \boldsymbol{\Sigma}_{\boldsymbol{dyn}}(\boldsymbol{r},\omega)\right\} \times \begin{bmatrix}\delta\phi_1(\boldsymbol{r},\omega)\\ \delta\phi_2(\boldsymbol{r},\omega)\end{bmatrix} = \begin{bmatrix}S_1(\boldsymbol{r},\omega)\\ S_2(\boldsymbol{r},\omega)\end{bmatrix}, \tag{1}$$

here $\delta\phi_1(\boldsymbol{r},\omega)$ and $\delta\phi_2(\boldsymbol{r},\omega)$ are the induced neutron noise in the fast and thermal groups, respectively.

$$\boldsymbol{D}(\boldsymbol{r}) = \begin{bmatrix}D_{1,0}(\boldsymbol{r}) & 0\\ 0 & D_{2,0}(\boldsymbol{r})\end{bmatrix}, \tag{2}$$

$$\boldsymbol{\Sigma}_{\boldsymbol{dyn}}(\boldsymbol{r},\omega) = \begin{bmatrix} -\left(\Sigma_{a,1,0}(\boldsymbol{r}) + \frac{i\omega}{\nu_1} + \Sigma_{r,0}(\boldsymbol{r}) - \frac{\upsilon\Sigma_{f,1,0}(\boldsymbol{r})}{k_{eff}}\left(1 - \frac{i\omega\beta}{i\omega+\lambda}\right)\right) & \frac{\upsilon\Sigma_{f,2,0}(\boldsymbol{r})}{k_{eff}}\left(1 - \frac{i\omega\beta}{i\omega+\lambda}\right)\\ \Sigma_{r,0}(\boldsymbol{r}) & -\left(\Sigma_{a,2,0}(\boldsymbol{r}) + \frac{i\omega}{\nu_2}\right)\end{bmatrix}, \tag{3}$$

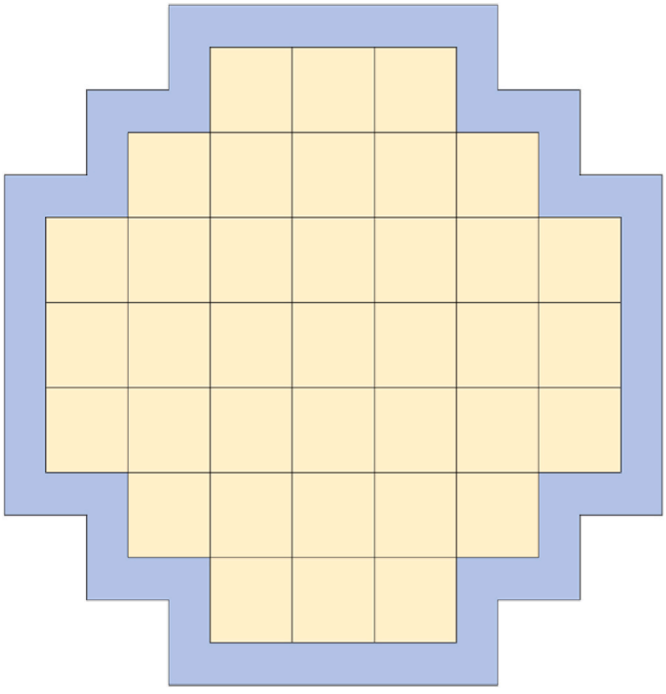

Fig. 1. Radial 2D layout of the SMR core showing the fuel assemblies in yellow and the core reflector in blue.

$$\Sigma_{r,0}(\boldsymbol{r}) = \Sigma_{s0,1\to2}(\boldsymbol{r}) - \Sigma_{s0,2\to1}(\boldsymbol{r})\frac{\phi_{2,0}(\boldsymbol{r})}{\phi_{1,0}(\boldsymbol{r})}. \tag{4}$$

The notations are standard and can be found in (Mylonakis et al., 2021).

The neutron noise source on the right-hand side of Eq. (1) is calculated by user-defined perturbations of absorption, fission and removal macroscopic cross-sections using the following equation:

$$\begin{bmatrix}S_1(\boldsymbol{r}',\omega)\\ S_2(\boldsymbol{r}',\omega)\end{bmatrix} = \boldsymbol{\phi}_{\boldsymbol{r}}(\boldsymbol{r}')\delta\Sigma_r(\boldsymbol{r}',\omega) + \boldsymbol{\phi}_{\boldsymbol{a}}(\boldsymbol{r}')\begin{bmatrix}\delta\Sigma_{a,1}(\boldsymbol{r}',\omega)\\ \delta\Sigma_{a,2}(\boldsymbol{r}',\omega)\end{bmatrix} + \boldsymbol{\phi}_{\boldsymbol{f}}(\boldsymbol{r}',\omega)\begin{bmatrix}\delta\upsilon\Sigma_{f,1}(\boldsymbol{r}',\omega)\\ \delta\upsilon\Sigma_{f,2}(\boldsymbol{r}',\omega)\end{bmatrix}, \tag{5}$$

$$\boldsymbol{\phi}_{\boldsymbol{r}}(\boldsymbol{r}) = \begin{bmatrix}\phi_{1,0}(\boldsymbol{r})\\ -\phi_{1,0}(\boldsymbol{r})\end{bmatrix}, \tag{6}$$

$$\boldsymbol{\phi}_{\boldsymbol{a}}(\boldsymbol{r}) = \begin{bmatrix}\phi_{1,0}(\boldsymbol{r}) & 0\\ 0 & \phi_{2,0}(\boldsymbol{r})\end{bmatrix}, \tag{7}$$

$$\boldsymbol{\phi}_{\boldsymbol{f}}(\boldsymbol{r},\omega) = \begin{bmatrix} -\frac{\phi_{1,0}(\boldsymbol{r})}{k_{eff}}\left(1 - \frac{i\omega\beta}{i\omega+\lambda}\right) & -\frac{\phi_{2,0}(\boldsymbol{r})}{k_{eff}}\left(1 - \frac{i\omega\beta}{i\omega+\lambda}\right)\\ 0 & 0\end{bmatrix}. \tag{8}$$

where $\delta\Sigma_{x,g}(\boldsymbol{r}',\omega)$ is the perturbation in cross-section x of group g at location $\boldsymbol{r}'$ at frequency ω represented in the frequency domain.

Since the reactor noise is given in the frequency domain as the Fourier transform of the time domain signal, the reactor noise $\delta\phi_g(\boldsymbol{r},\boldsymbol{\omega})$ is a complex number. The complex number contains the amplitude representing the magnitude of fluctuations and the phase indicating their time variation.

The SMR is modelled in CORE SIM + where each assembly is divided into 4x4 nodes. The core is surrounded by a reflector of 2 nodes, resulting in the final 2D core represented as a 32x32 mesh grid as shown in Fig. 1. Using CORE SIM+, we calculate the static neutron flux and reactor neutron noise for the fast and thermal groups.

2.2. Absorber of Variable Strength (AVS) noise source

A specific type of perturbation, the Absorber of Variable Strength (AVS), is the focus of this study. Although AVS is an artificial type of perturbation, it provides a well-defined and theoretically significant test case for developing models and methods that can be applicable to broader anomaly detection scenarios.

To model the AVS perturbation, we first solve the Green's function by treating a spatial Dirac delta function as the neutron noise source. We apply this to a single node in the reactor system such that Eq. (1) becomes:

$$\left\{\nabla.[\mathbf{D}(\mathbf{r})\nabla] + \boldsymbol{\Sigma}_{\mathbf{dyn}}(\mathbf{r},\boldsymbol{\omega})\right\} \times \begin{bmatrix}G_{g\to1}(\mathbf{r},\mathbf{r}',\omega)\\ G_{g\to2}(\mathbf{r},\mathbf{r}',\omega)\end{bmatrix} = \begin{bmatrix}\delta(\mathbf{r}\text{-}\mathbf{r}')\\ 0\end{bmatrix}_{g=1} \text{ or } \begin{bmatrix}0\\ \delta(\mathbf{r}\text{-}\mathbf{r}')\end{bmatrix}_{g=2}. \tag{9}$$

for a perturbation in the fast group and thermal group, respectively.

This Green's function response represents the system's noise response to a localized perturbation. To model an AVS response, we utilize the Green's function response in combination with neutron noise sources, which are represented by fluctuations in various neutron cross-sections within the system. Each type of cross-section perturbation has a different effect on the neutron noise source as observed in Eq. (5), and thus has a different effect on the resulting neutron noise.

To calculate the neutron noise from different perturbations in one location, we use the Green's function response at this location by applying the following equation:

$$\begin{bmatrix}\delta\phi_1(\boldsymbol{r},\omega)\\ \delta\phi_2(\boldsymbol{r},\omega)\end{bmatrix}=\begin{bmatrix}\int\{G_{1\to1}(\boldsymbol{r},\boldsymbol{r}',\omega)S_1(\boldsymbol{r}',\omega)+G_{2\to1}(\boldsymbol{r},\boldsymbol{r}',\omega)S_2(\boldsymbol{r}',\omega)\}d^3\boldsymbol{r}'\\ \int\{G_{1\to2}(\boldsymbol{r},\boldsymbol{r}',\omega)S_1(\boldsymbol{r}',\omega)+G_{2\to2}(\boldsymbol{r},\boldsymbol{r}',\omega)S_2(\boldsymbol{r}',\omega)\}d^3\boldsymbol{r}'\end{bmatrix} \tag{10}$$

By studying AVS cases, we can explore the fundamental relationship between reactor neutron noise and perturbation location. By varying the source location and the neutron noise sources of the AVS perturbations, we generate a dataset of various AVS scenarios to be the basis for training and evaluating the machine learning framework presented in this paper.

3. Physics-based considerations about neutron noise in water-cooled SMRs

3.1. Theoretical considerations

Neutron noise arises from small, time-dependent fluctuations in the static neutron flux due to perturbations in reactor parameters which require analyzing and interpreting neutron noise in SMR systems. In this section, we will decompose the reactor noise into its components to better understand its behavior in SMRs.

3.1.1. Point-kinetic and non-point-kinetic components

Reactor neutron noise in nuclear reactors can be decomposed into two principal components: the point kinetic (PK) component and the deviation from point-kinetic component (the non-point-kinetic component). These components play distinct roles in describing the system response to perturbations.

The point kinetic component of the reactor noise has the same spatial distribution as the static neutron flux. This means that it lacks any sensitivity to the type or location of the perturbation within the reactor in terms of spatial response. While its amplitude reflects the reactor overall reactivity effect of the noise source, it does not provide any localized information that could be used to identify the nature or position of noise sources. The factorized form of the reactor noise is given by (Pázsit and Demazière, 2010):

$$\delta\phi_g(\boldsymbol{r},\omega)=\phi_{g,0}(\boldsymbol{r})\frac{\delta P(\omega)}{P_0}+P_0\,\delta\psi_g(\boldsymbol{r},\omega), \tag{11}$$

where the first term on the right-hand side is the point kinetic component represented by the multiplication of the static flux and the integral value expressed by:

$$\frac{\delta P(\omega)}{P_0}=\frac{\int\left[\frac{1}{v_1}\phi^\dagger_{1,0}(\boldsymbol{r})\delta\phi_1(\boldsymbol{r},\boldsymbol{\omega})+\frac{1}{v_2}\phi^\dagger_{2,0}(\boldsymbol{r})\delta\phi_2(\boldsymbol{r},\omega)\right]d\boldsymbol{r}}{\int\left[\frac{1}{v_1}\phi^\dagger_{1,0}(\boldsymbol{r})\phi_{1,0}(\boldsymbol{r})+\frac{1}{v_2}\phi^\dagger_{2,0}(\boldsymbol{r})\phi_{2,0}(\boldsymbol{r})\right]d\boldsymbol{r}}. \tag{12}$$

The point kinetic term can be calculated by an alternative method using the reactivity of the noise and the zero-power reactor transfer function as shown in the following equations (Demazière and Andhill, 2005; Pázsit and Demazière, 2010):

$$\delta P(\omega)=P_0\,G_0(\omega)\delta\rho(\omega) \tag{13}$$

$$G_0(\omega)=\frac{1}{i\omega\left(\Lambda_0+\frac{\beta}{i\omega+\lambda}\right)}. \tag{14}$$

The non-point-kinetic component, represented by the second term on the right-hand side of Eq. (11), consists of the non-point kinetic shape function $\delta\psi_g(\boldsymbol{r},\omega)$ multiplied by the static reactor power amplitude. This term contains valuable information about the characteristics of the perturbation. This component is highly dependent on the location and type of perturbation, making it the primary focus for applications such as anomaly detection and noise source localization.

In smaller systems like SMRs, the point kinetic component becomes relatively stronger than the non-point-kinetic component compared to large systems (Demazière et al., 2022; Pázsit and Demazière, 2010). This dominance of the PK component makes it more challenging to extract meaningful information about anomalies and noise sources. Consequently, detecting and localizing perturbations in SMRs becomes a more problematic task than in larger reactor systems.

3.1.2. Global and local components

An alternative representation for understanding reactor noise involves decomposing it into a global component with a long spatial relaxation length and a local component with a short relaxation length. The global component represents the reactor-wide effects of noise, which typically propagates through the entire core. On the other hand, due to the short relaxation length of the local component, its effect does not extend beyond the vicinity of the noise source. In a one-dimensional (1D) homogeneous reactor, the global and local components for the reactor noise — denoted as $\delta\phi_\mu$ and $\delta\phi_\nu$, respectively — are given by:

$$\begin{bmatrix}\delta\phi_1(\boldsymbol{r},\omega)\\ \delta\phi_2(\boldsymbol{r},\omega)\end{bmatrix}=\begin{bmatrix}1\\ c_\mu(\omega)\end{bmatrix}\delta\phi_\mu(\boldsymbol{r},\omega)+\begin{bmatrix}1\\ c_\nu(\omega)\end{bmatrix}\delta\phi_\nu(\boldsymbol{r},\omega), \tag{15}$$

$$c_\mu(\omega)=\frac{\Sigma_{r,0}}{\Sigma_{a,2,0}+\frac{i\omega}{v_2}+D_{2,0}\mu^2}, \tag{16}$$

$$c_\nu(\omega)=\frac{\Sigma_{r,0}}{\Sigma_{a,2,0}+\frac{i\omega}{v_2}-D_{2,0}\nu^2}, \tag{17}$$

$$\begin{vmatrix}-D_{2,0}b^2(\omega)-\Sigma_1(\omega) & v\Sigma_{f,2,0}\left(1-\frac{i\omega\beta}{i\omega+\lambda}\right)\\ \Sigma_{r,0} & -D_{2,0}b^2(\omega)-\left(\Sigma_{a,2,0}+\frac{i\omega}{v_2}\right)\end{vmatrix}=0. \tag{18}$$

Eq. (15) has a non-trivial solution when the following determinant is equal to zero (Demazière and Andhill, 2005):

This equation has two roots for b^2, namely μ^2 and $-\nu^2$.

The interplay between these components determines the spatial characteristics of neutron noise and influences the strategies employed for noise source localization.

3.2. Numerical investigations

In an SMR, the core size is significantly smaller than in a conventional reactor, leading to different physical and operational characteristics. The compact geometry affects the spatial distribution of the neutron flux and alters the balance between the point-kinetic and non-point-kinetic components of the noise. In this study, we aim to highlight the effect of the reactor core size on the reactor noise behavior and understand possible challenges that arise in localizing noise sources.

For demonstration purposes, we study two 1D homogenous reactors, a large reactor of size $a=344$ cm and a reactor of size $a=172$ cm, respectively. We consider two local cases of 1 Hz AVS sources of 5 % perturbation in the thermal absorption cross-section $\delta\Sigma_{a,2}=5\%\ \Sigma_{a,2,0}$, one located at the center of the core and the second located at a distance $-a/4$ from the core center.

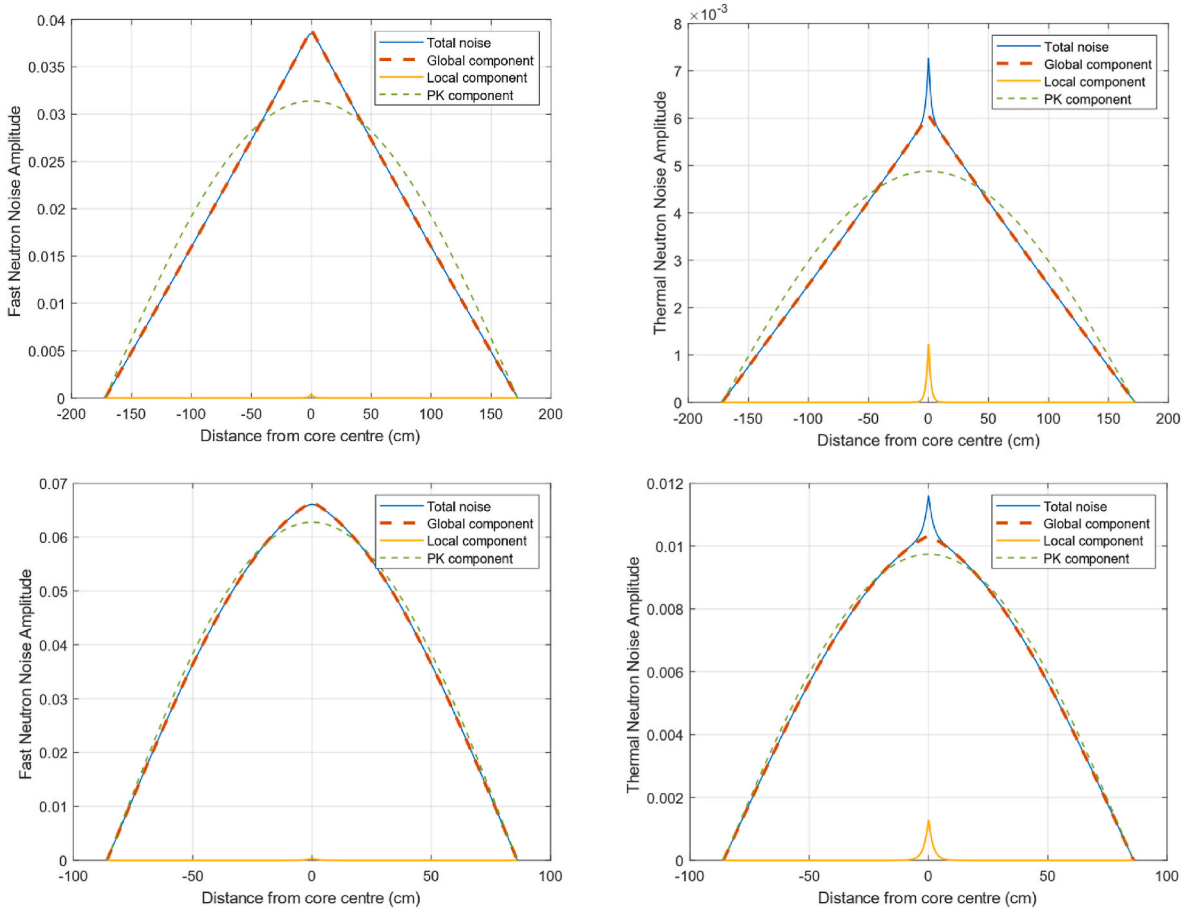

Fig. 2. Reactor noise amplitude for a central perturbation in a 1D homogenous core and its point-kinetic, local and global components. The right plots are for the fast group, the left plots are for the thermal group, the upper plots are for the large core, and the lower plots are for the small core.

The cases with the central and non-central AVS are demonstrated in Figs. 2 and 3, respectively, where the total reactor noise amplitude is shown in the fast and thermal groups for both reactors in comparison with the point-kinetic component, global component and local component. We can observe the difference between the reactor noise shape in the large and small reactors that arises from the distinction between the levels of the point-kinetic component. The deviation of the total noise from point-kinetics is clearly visible, and it can be noted that the reactor noise shape in the small reactor follows a similar behavior as the point-kinetic component, although it is slightly shifted in the second case due to the off-center perturbation. This distinction highlights the challenge in the detection of the neutron noise source in small-size reactors compared to conventional large reactors.

It can be seen in Fig. 2 that the effect of the global component in the large and small reactors spreads throughout the reactor and peaks at the noise source location, dominating the reactor noise response. However, in the non-central perturbation case shown in Fig. 3, the peak effect is less pronounced in the small reactor while it is clearly visible in the large reactor. By examining the local component response, we can find that it is only visible in the neighborhood of the source due to its short relaxation length.

Since the global component is visible far from the noise source location, it is the component responsible for providing information about the noise source from remote neutron detectors. It is also worth noting that the local component is visibly stronger in the thermal group of reactor noise than in the fast group, giving an advantage to the thermal noise in localizing noise sources in the vicinity of the noise origin. Therefore, in the vicinity of the noise source, the local component plays a significant role, especially with thermal neutrons.

Since the point-kinetic component contains no information about the location of the AVS source, it is beneficial to account for the deviation of the total noise as well as its components, i.e. the global and local components, from the point-kinetic component. We represent this deviation as the fraction between each component and the point-kinetic component: $\frac{\delta\phi_g(r,\omega)}{\delta\phi_{g_{pk}}(r,\omega)}$, $\frac{\delta\phi_{\mu_g}(r,\omega)}{\delta\phi_{g_{pk}}(r,\omega)}$, and $\frac{\delta\phi_{\varepsilon_g}(r,\omega)}{\delta\phi_{g_{pk}}(r,\omega)}$. The deviation from point-kinetics is estimated from the deviation of those quantities from unity. This is observed in Fig. 4 for the central AVS and in Fig. 5 for the off-central AVS, where it is clear that for all components it is much more significant in the large core than in the small core. To quantify this deviation, we subtract unity to estimate the distance of the total noise and the global component from the point-kinetic component according to:

$$\frac{1}{a}\int_{-\frac{1}{2}a}^{\frac{1}{2}a}\left|\frac{\delta\phi_{g_c}(x,\omega)}{\delta\phi_{g_{pk}}(x,\omega)}-1\right|dx\,. \tag{19}$$

where $\delta\phi_{g_c}$ is the reactor noise 'c' component for group g neutrons. 'c' can be the total noise, the global component, or the local component.

The closer to zero this measure is, the larger point-kinetics prevails, and the more difficult it is to make efficient diagnostics. Since the local component is significantly smaller than the point-kinetic component, its deviation from point kinetics is nearly zero. Thus, subtracting unity to account for this deviation is not representative of the local component. Such a metric is thus not reported hereafter. Table 1 shows the values of the deviation. The values confirm the larger quantity of information available in the large reactor than the smaller reactor. We can also confirm that the total reactor noise in the thermal group contains higher deviation from point-kinetics, offering more information compared to

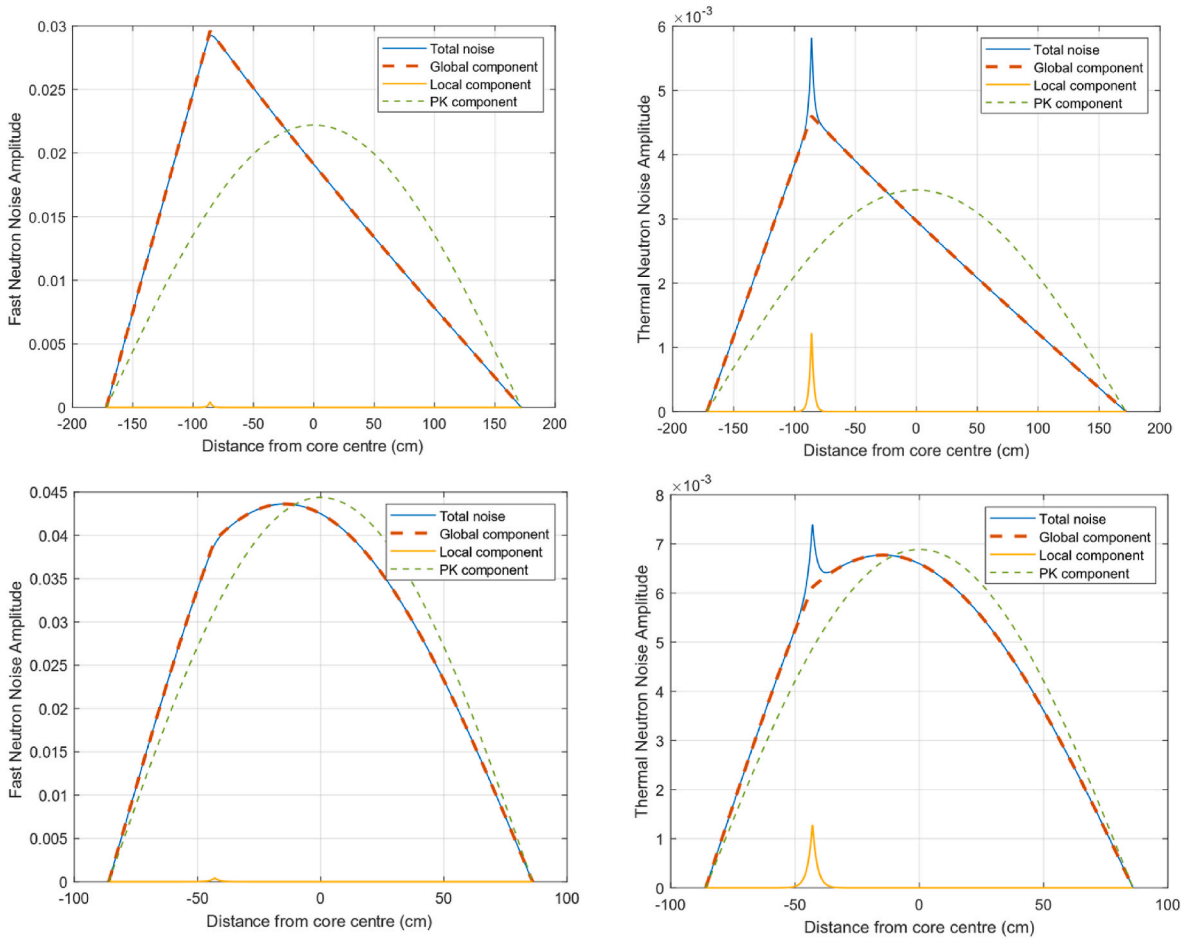

Fig. 3. Reactor noise amplitude for a non-central perturbation in a 1D homogenous core and its point-kinetic, local and global components. The right plots are for the fast group, the left plots are for the thermal group, the upper plots are for the large core, and the lower plots are for the small core.

the fast group. Notably, the global component deviation from point kinetics is comparable in both fast and thermal groups. This suggests that the additional information provided by the total thermal noise primarily arises from the local component.

The numerical findings emphasize the need for advanced methods, such as machine learning, to effectively interpret the reactor noise response among the strong influence of point kinetic effect. In addition, the observation of thermal noise containing more deviation from point kinetics than the fast neutrons can be used to our advantage. These results lay the foundation for the subsequent sections, which explore the application of machine learning for neutron noise source localization in an SMR.

4. Noise source detection using machine learning

In this section, we present our approach for localizing AVS sources in an SMR core using machine learning. In this method, we use the complex-valued relative reactor noise as input. The relative noise is calculated by dividing the reactor noise generated by CORE SIM+ in the frequency domain by the static flux. We train our model using simulated data since it is the only available training resource that enables node-level control over perturbation scenarios. We use the relative reactor noise as practically the measurement of this value eliminates the need to know the detector efficiency. This has some practical implications in terms of the implementation of noise techniques in reactors. In addition, the relative noise emphasizes the deviation of the neutron noise from the static flux (Hursin et al., 2023). We apply a convolutional neural network (CNN) (LeCun et al., 2015) to our data to capture the space information in the reactor noise and detect the locations of one or more AVS sources. CNNs are particularly well-suited for this task, as the reactor noise data can be represented in an image-like format, enabling the network to effectively learn and exploit spatial features and extract relationships between neighboring points.

In this work, we restrict the study on perturbations with a frequency of 1 Hz. This frequency falls within the typical range of possible perturbation frequencies, which spans approximately from 0.1 Hz to 25 Hz. Furthermore, 1 Hz falls within the frequency plateau region of the neutron noise spectrum, where similar perturbations with different frequencies induce similar neutron noise amplitude distributions with minor phase variations. Therefore, selecting 1 Hz provides a practical baseline for the ongoing analysis.

4.1. Data processing

Processing complex values for the CNN poses a challenge since the complex numbers need to be represented as the amplitude of the relative reactor noise response and its phase angle. Normalization of input values to artificial neural networks (ANNs) is a common practice to enhance convergence and training stability by ensuring that all features have a similar scale. Normalization of phase angles is shown to be problematic because of their periodic nature. Phase angles measured in degrees are typically found between 0° and 360°, where 0° and 360° represent the same phase angle, only differing by a full cycle. Treating these values linearly, we can see that they are numerically far apart, even though they represent the same angle. Standard normalization techniques fail to account for this cyclic nature and will lead to incorrect angle

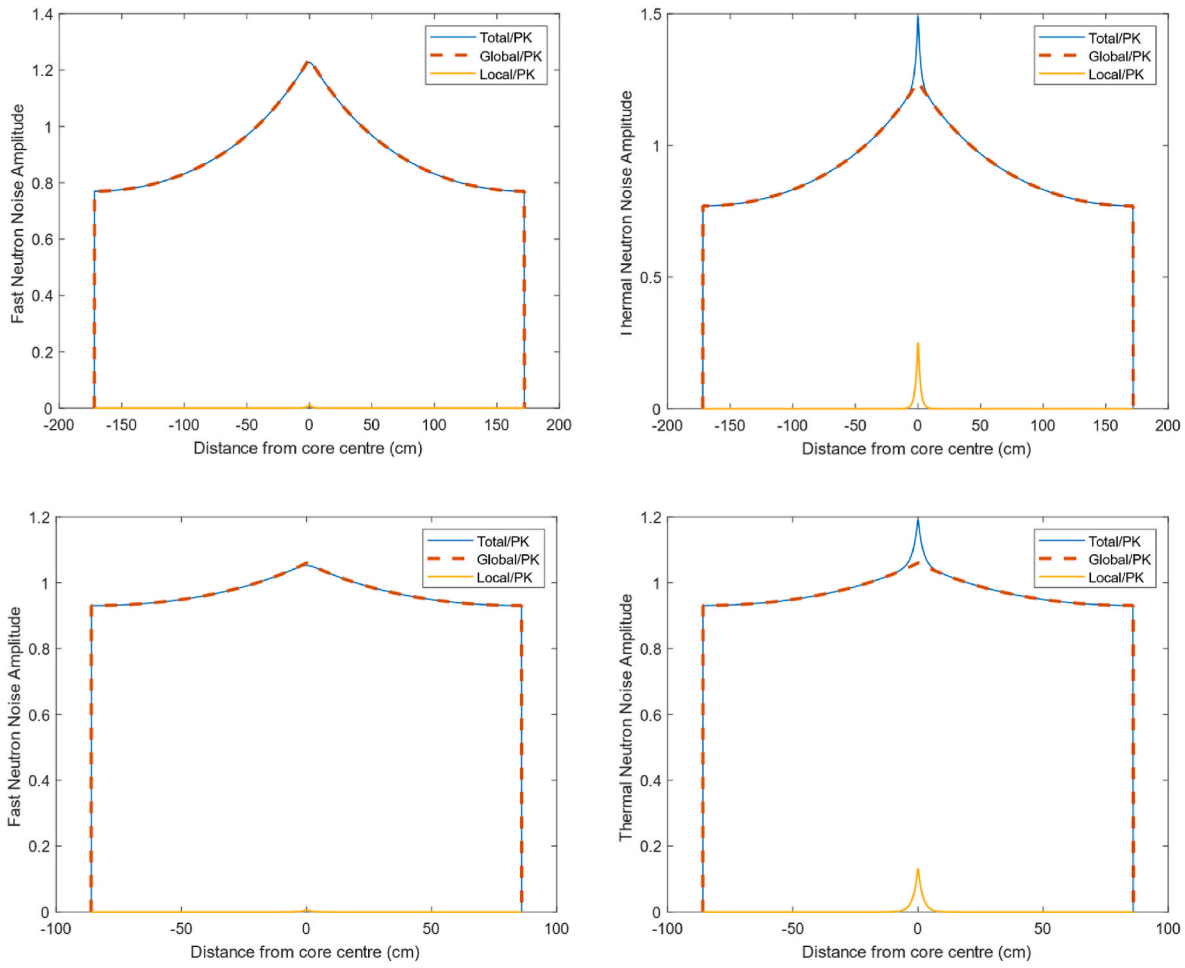

Fig. 4. Deviation of the total noise and its global and local components from point-kinetic component represented as fractions divided by the point-kinetic component in the central AVS case. The right plots are for the fast group, the left plots are for the thermal group, the upper plots are for the large core, and the lower plots are for the small core.

representations. To address this problem, we represent the phase angles using the cosine and sine of the phase angles. The input used for our model has 3 channels per energy group.

- One channel for the amplitude of the relative reactor noise where the amplitude is normalized using min-max normalization, thus represented by values between 0 and 1.
- Two channels representing the angle as the cosine and sine of the relative reactor noise phase, respectively. Since the cosine and sine naturally lie between -1 and 1, no further normalization is needed. This ensures that the angular information is maintained in the model input.

This three-channel input per energy group allowed the CNN to extract the features and properties of the neutron noise in the system required for the localization of available AVS perturbations.

In this section, we considered three cases of input data to our model.

i. A case using only relative fast-group reactor noise as input (3 channels)
ii. A case using only relative thermal-group reactor noise as input (3 channels)
iii. A case using both relative fast and thermal groups reactor noise as input (6 channels)

4.2. Model architecture

The CNN aims to analyze the neutron noise distribution throughout the 2D SMR for spatial pattern recognition. The model input consists of a 2D mesh grid with the size (32 x 32) representing the relative reactor noise distribution throughout the core using 3 channels per energy group as described above. One convolutional hidden layer is used by applying 2048 filters of 3x3 size. The convolutional layer extracts information from the input using 3x3 kernel-size filters with 1-node stride. This layer utilizes a 'ReLU' activation function to capture the nonlinearity in the system allowing to capture the spatial dependencies within the data (Dubey et al., 2022). A convolutional output layer is used to reconstruct the shape of system (32 x 32 nodes), where each node corresponds to its original location in the 2D system. Each node is assigned a binary classification label: '0′ indicating no perturbation and '1′ indicating the presence of a perturbation. A 'Sigmoid' activation function is used such that each node holds the probability of the corresponding location having an AVS perturbation source. The used model architecture is demonstrated in Fig. 6.

The model is trained using the Adaptive Moment Estimation 'AdaM' optimizer (Kingma and Ba, 2015) with an initial learning rate of 0.0005 to minimize a binary cross-entropy loss function given by (Terven et al., 2023):

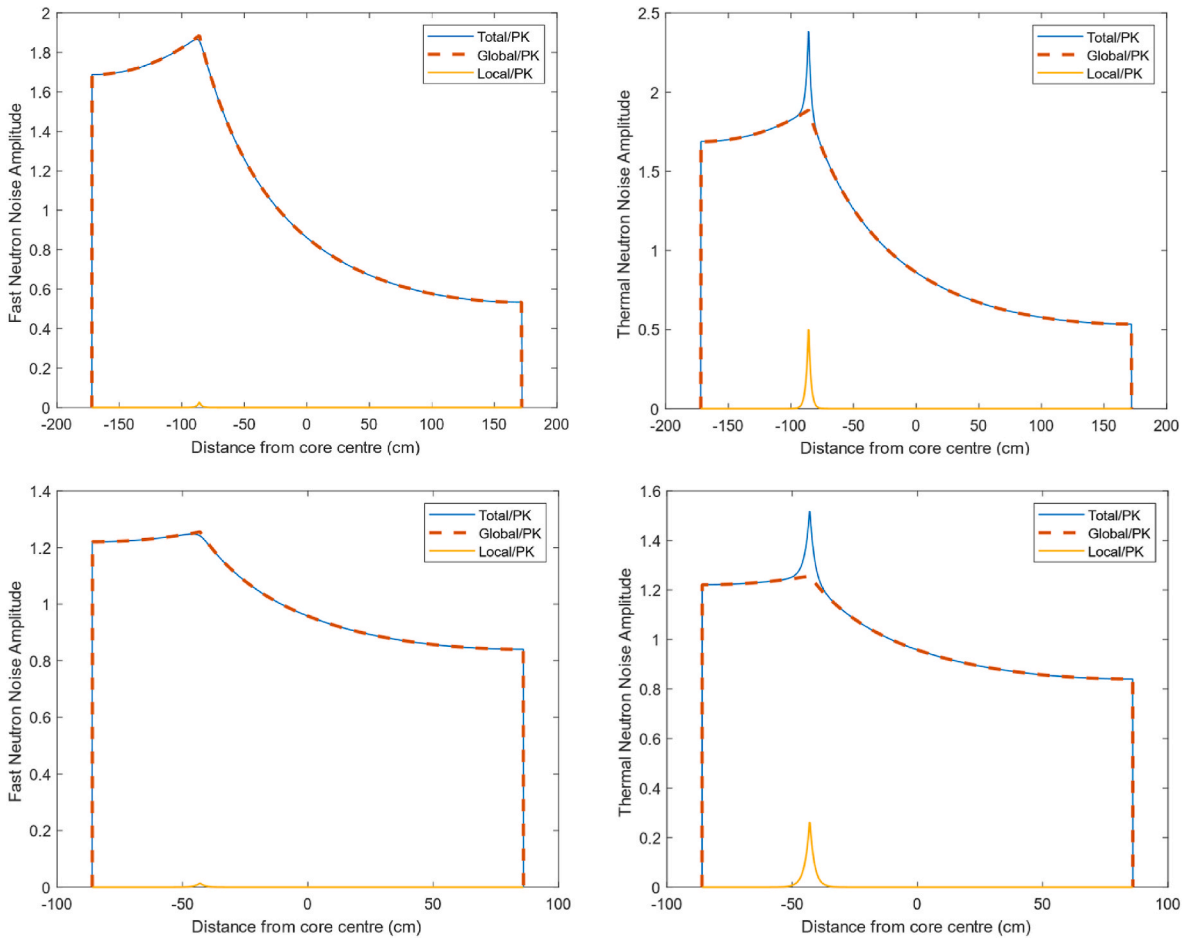

Fig. 5. Deviation of the total noise and its global and local components from point-kinetic component represented by fractions divided by the point-kinetic component in the central AVS case. The right plots are for the fast group, the left plots are for the thermal group, the upper plots are for the large core, and the lower plots are for the small core.

Table 1
Values quantifying the deviation of the total and global component from point-kinetic (PK) component.

Case		Small reactor		Large reactor	
		$\delta\phi_g(r,\omega)$	$\delta\phi_{\mu_g}(r,\omega)$	$\delta\phi_g(r,\omega)$	$\delta\phi_{\mu_g}(r,\omega)$
Central AVS	*Fast (g = 1)*	0.0438	0.0440	0.1472	0.1474
Central AVS	*Thermal (g = 2)*	0.0467	0.0438	0.1501	0.1473
Non-central AVS	*Fast (g = 1)*	0.1417	0.1420	0.4436	0.4439
Non-central AVS	*Thermal (g = 2)*	0.1478	0.1420	0.4497	0.4440

Binary crossentropy =

$$-\frac{1}{N}\sum_{i=1}^{N}\left[y_{true}\log\left(y_{pred}\right)+(1-y_{true})\log\left(1-y_{pred}\right)\right]. \quad (20)$$

where N is the total number of locations (32x32) in one sample. y_{true} is the actual value for one location given by the ground truth; either a '0' representing no AVS source or a '1' representing an AVS source. y_{pred} is the value predicted by the model for one location, given by a value between 0 and 1, showing the confidence of the model in the presence of an AVS source in the corresponding location.

During training, the model minimizes the loss function using the training dataset in batches of 100 samples and for 100 epochs. Different hyperparameters are tested for each case through grid search with cross-validation and the optimal values are selected. The hyperparameters mentioned in the text are for the case using relative thermal reactor noise only.

4.3. Training and validation datasets

The training and validation datasets for the CNN model are generated by simulating multiple cases of AVS perturbation sources. Our dataset is divided into two types of cases.

1. Cases with a single AVS source present in the 2D SMR. 349,872 cases of this type are present in the dataset, covering multiple cases for all possible locations of AVS sources in the system with different fast and thermal source intensities. These cases are fundamental to capture the locations where neutron noise sources could be present with varying intensities. Each sample input is represented using the relative reactor noise distribution by three channels (six channels in case of fast and thermal input), and the output is represented by the 32x32 grid of zeros and one in the location of the AVS source.
2. Cases with two AVS sources present simultaneously in the system. For this type, a similar number of samples as the first type is generated for the dataset such that the model can learn from balanced data to avoid bias towards a certain type and to achieve more robust results. The presence of this type in the dataset is

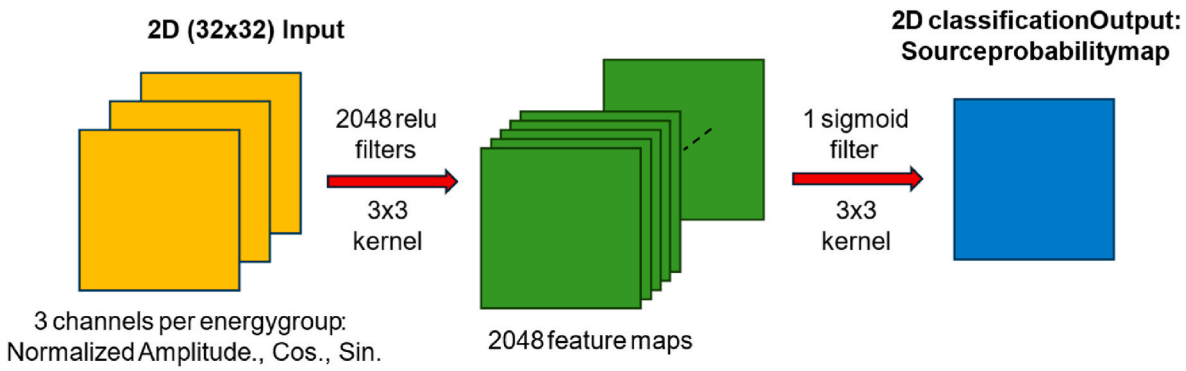

Fig. 6. Localization model architecture using full neutron noise.

essential to enable the model to capture the effect of having more than one source in the system and recognize the relation between them. The cases cover all possible combinations of two simultaneous AVS sources available in the 2D system. Each AVS source has independent fast and thermal source intensities and phases.

The dataset is limited to cases with one and two AVS sources to enable the model to learn the complex relationships between perturbations through a large number of relatively simple scenarios. This approach is particularly advantageous, as the model is designed to predict an arbitrary number of AVS sources in the system without requiring training samples for every possible number of sources. This is shown in further detail hereafter.

By studying practical cases of perturbations in the SMR system, we observe that the fast source intensity is usually 10 orders of magnitude higher than the thermal source intensity. However, less probable cases have a higher thermal source intensity than the fast source intensity. Based on this observation, our AVS sources are modelled by randomly sampling the thermal sources from a narrower range than those used for the fast sources. This resulted in 99.5 % of the cases having a higher fast source intensity and only 0.5 % of the cases having a higher thermal source intensity, representing a distribution of cases closer to reality.

During the training phase, 90 % of the dataset is used for training, while the remaining 10 % was used for validation purposes.

4.4. Numerical results

After training our CNN binary classification model, we test its performance on unseen cases for one and two AVS sources. We also aim to test our model's ability to generalize and detect more than two AVS sources. Since we are interested in the predicted source positions, i.e., the classified '1's, which are a minority in the 32x32 grid space, it is informative to use typical classification performance metrics such as the recall, precision, and their harmonic mean, i.e., F1 score. The definitions of these metrics are as follows (Terven et al., 2023):

$$Recall = \frac{True\ positive}{True\ positive + False\ negative}, \tag{21}$$

$$Precision = \frac{True\ positive}{True\ positive + False\ positive}, \tag{22}$$

$$F1\ score = \frac{2^{*}\ Precision^{*}\ Recall}{Precision + Recall}. \tag{23}$$

where a true positive is a '1' predicted where there is an actual source, a true negative is a '0' predicted where there is no source, a false positive is a '1' predicted where there is no source, and a false negative is a '0' predicted where there is a source.

As mentioned earlier, the model is trained using a binary cross-entropy loss function, which optimizes both recall and precision by minimizing the discrepancy between predicted and true classifications. To assess the consistency of the model, Table 2 reports the recall and precision values across the training, validation, and test datasets for the relative thermal neutron noise input model. The close values of the metrics across the three datasets for 1 and 2 sources indicate stable performance and suggest that the model generalizes well without signs of overfitting.

In section 3, we showed that the thermal noise includes more information deviating from the point kinetic component, thus holding more information about the noise source. In Fig. 7, we present the difference in performance for the location detection model for relative fast-group, relative thermal-group, and relative fast and thermal groups neutron noise cases. The results show that the thermal reactor noise has higher recall and F1 score in comparison to the fast-group reactor noise, in addition to a comparable precision for different number of sources. These results support our previous conclusion that thermal noise outperforms fast noise in localization of the noise source. Using relative fast-group neutron noise in addition to thermal noise is computationally much more expensive than using only one type. Despite that it holds information from both energy groups, we can observe that it does not contribute significantly to better performance. Based on these considerations, we select relative thermal neutron noise for our analysis.

The relative thermal neutron noise model is highly accurate in predicting the location of one AVS source, with recall, precision, and F1 score very close to unity. For two sources, the model also performs very well with a slight decrease in recall, precision, and F1 score. The model accurately identifies both source locations with minimal errors. We also test our CNN model on cases with multiple AVS sources (up to 10 perturbations at a time). The model shows a slightly decreasing trend in the performance metrics as the number of perturbation sources increase. However, the performance remains very good, even up to 10 AVS sources with a recall value around 99 %, precision around 99.9 %, and F1 score 99.4 %. This demonstrates the robustness of the model in handling multiple AVS sources with minimal false positives and negatives.

Table 2
Training, validation, and testing performance for cases with 1 and 2 sources.

	Training		Validation		Testing	
	1 source	2 sources	1 source	2 sources	1 source	2 sources
Recall (%)	100.00	99.96	100.00	99.92	100.00	99.97
Precision (%)	100.00	99.99	100.00	99.98	99.99	99.96

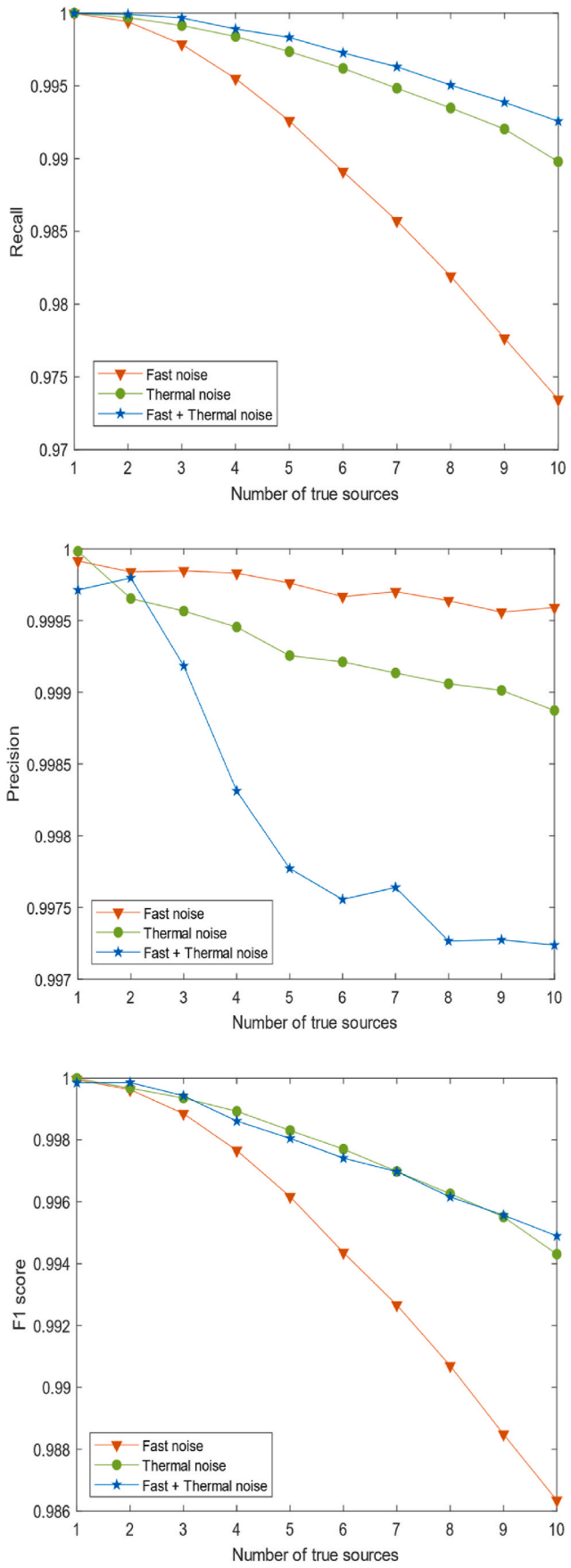

Fig. 7. Metrics for the performance using relative thermal-group, fast-group, and thermal-group + fast-group noise as input for location detection model.

5. Impact of limited instrumentation on reactor core

In this section, we introduce the challenge of instrumentation availability in a reactor core and its impact on the ability of the model to detect accurate AVS source locations. In practice, reactor noise information is only available at discrete locations inside the core where reactor noise detectors are placed. In this work, we investigate the performance of our model using different densities of available detectors to approximate the performance of our model to realistic operating conditions.

In an actual reactor core, neutron detectors cannot be available at every point in the system due to geometric, cost, and technical limitations. In a PWR, the number of detector is typically low to minimize interference with reactor operations, and radiation exposure. Accordingly, our 32 x 32 grid should contain sparse information where the detectors are present and zeros in unavailable locations. In this section, we evaluate the impact of reduced availability of neutron noise measurements on the accuracy and robustness of AVS source localization.

5.1. Model architecture for limited data cases

To adjust our model to accommodate missing information, we apply a two-model pipeline approach for the study. The pipeline takes sparse reactor noise data as input, reconstructs the full noise information, then localizes the AVS sources.

i. Model 1: Noise reconstruction model

The first model of the pipeline is designed to take spatial reactor noise information from the available sparse locations and predict the full reactor noise map. The model follows an encoder-decoder architecture (Ronneberger et al., 2015) with convolutional layers and inception blocks (Szegedy et al., 2016) optimized to infer the missing values using spatial dependencies in the 32 x 32 grid space.

The input layer for model 1 consists of 4 channels for 32 x 32 grid points. The first channel contains the reactor noise amplitude at the available sparse locations. The amplitude values in these available locations are normalized using minmax normalization and the remaining location values were set to zero. The second and third channels consist of the cosine and sine values of the noise phase angles, respectively. Similar to the first channel, the missing locations are set to zero. The fourth channel is a mask channel, containing unity at locations with available detectors and zeros everywhere else.

An encoder-decoder architecture is used to reconstruct the full noise representation. An encoder captures the features of the input data by compressing it into a dense representation called the latent space. The decoder then uses the latent space to reconstruct the full data representation including data points missing from the input. Our encoder-decoder model incorporates inception blocks, which allows the model to capture features by branching the same input layer on multiple scales by using different filter sizes. In addition to the multiscale extraction of the inception blocks, it allows the model to go deeper and learn more complex representations with reduced dimensionalities, leading to lower computational costs and improved efficiency. The architecture for model 1 is shown in Fig. 8.

The decoder has three branches to the output layer, each to reconstruct one of the 3 full channels (normalized amplitude, cosine phase, and sine phase) to be used next in the AVS localization model. The model is trained and validated by the same original samples used for training and validation of the localization model described in section 4. Thus, the model is trained on samples with 1 AVS and 2 AVS sources. The training of the model is done by minimizing the Mean Square Error (MSE) loss function given by (Terven et al., 2023):

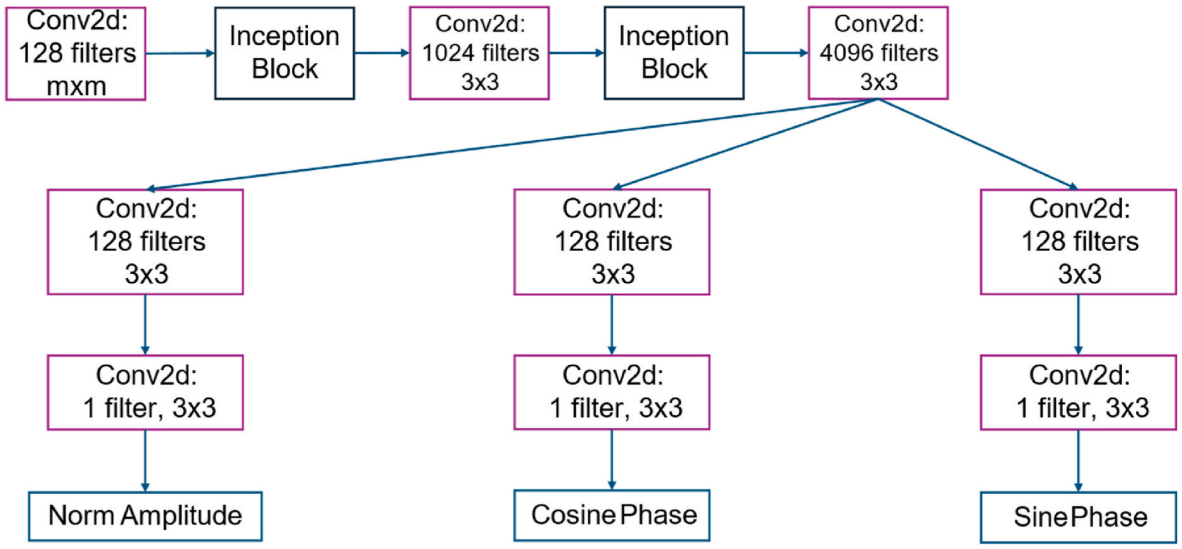

Fig. 8. Model 1 (reconstruction model) architecture. 'm' value differs for different detector densities. m = 3,5,7,9 for detector densities of 50,11,6,3 % respectively as shown in section 5.2.

$$\mathrm{MSE} = \frac{1}{N}\sum_{i=1}^{N}\left(y_{true} - y_{pred}\right)^2 . \tag{24}$$

ii. Model 2: AVS localization model

The AVS localization model takes the 3-channel full representation of the system and predicts the locations for present AVS sources in the 32 x 32 system grid. For this purpose, the model described in section 4 is used directly.

5.2. Cases of different densities of available instrumentation

To evaluate the performance of the pipeline concept with different densities of available instrumentation, we create 4 models with different levels of sparsity of instrumentation and test the performance of the full pipeline. As shown in Fig. 9, the selected detector locations are arranged symmetrically in all four models considered. However, since the neutron noise distribution in the system is inherently asymmetric — except in the special case where the perturbation is centrally located — each detector responds differently to the induced neutron noise, irrespective of its geometric symmetry.

i. **50 % Instrumentation coverage**

In this case, 50 % of the neutron noise data points (296 out of 592 in-core points) are available for reconstruction, which represents a relatively dense detector coverage. However, it shows the impact of removing half of the in-core information on the model.

ii. **11 % Instrumentation coverage**

For the second case, approximately 11 % of the noise data points (66 in-core points) are available, a scenario moving closer to realistic constraints. This case aims to determine the model's robustness when data is significantly reduced.

iii. **6 % Instrumentation coverage**

The third case represents one detector per assembly, covering 6 % of the core points (37 points) in the 32x32 grid. Although denser than realistic cases, it offers a useful intermediate step for evaluating the pipeline's performance with low-density instrumentation while retaining some spatial information.

iv. **3 % Instrumentation coverage**

To simulate a realistic scenario more closely, this configuration includes only one detector for every second assembly, representing 3 % coverage (21 points). This minimal instrumentation level tests the model's effectiveness with a very sparse, potentially feasible detector layout.

5.3. Numerical results

The pipeline performance is evaluated by measuring the precision, recall, and F1 score metrics when localizing AVS sources in unseen cases after using the pipeline.

5.3.1. Results for 50 % instrumentation coverage

The pipeline is tested on 592,000 cases with different number of AVS sources. With 50 % of the neutron noise data available, the reconstruction model is able to reconstruct the full relative thermal noise with test MSE shown in Table 3 for multiple AVS sources. The MSE values show the high ability of reactor noise reconstruction from 50 % available data with low error. Reconstruction error increases as the number of neutron noise sources in the system grows, reflecting the reduced ability to fully capture the complexity arising from the superposition of multiple sources. Nonetheless, the reconstruction remains highly effective even with a large number of noise sources. A reconstruction example containing 8 AVS sources is shown in Fig. 10. As described earlier, the model input contains zeros in locations with no detectors, however the zeros are removed from the figures for a clearer view. The figure shows the similarity between the reconstructed neutron noise and the true neutron noise, demonstrating the capability of inferring missing noise data points. The successful reconstruction can be attributed to the presence of the global information from the available detectors as well as the local information since there is a detector relatively close to all points inside the core. Retrieving global and local information enables the model to accurately capture the detailed behavior of the noise. Model 2 in the pipeline uses the reconstructed full noise to localize the AVS sources.

Given the limited information available in the input data, it becomes important to adopt a proximity range when evaluating the final

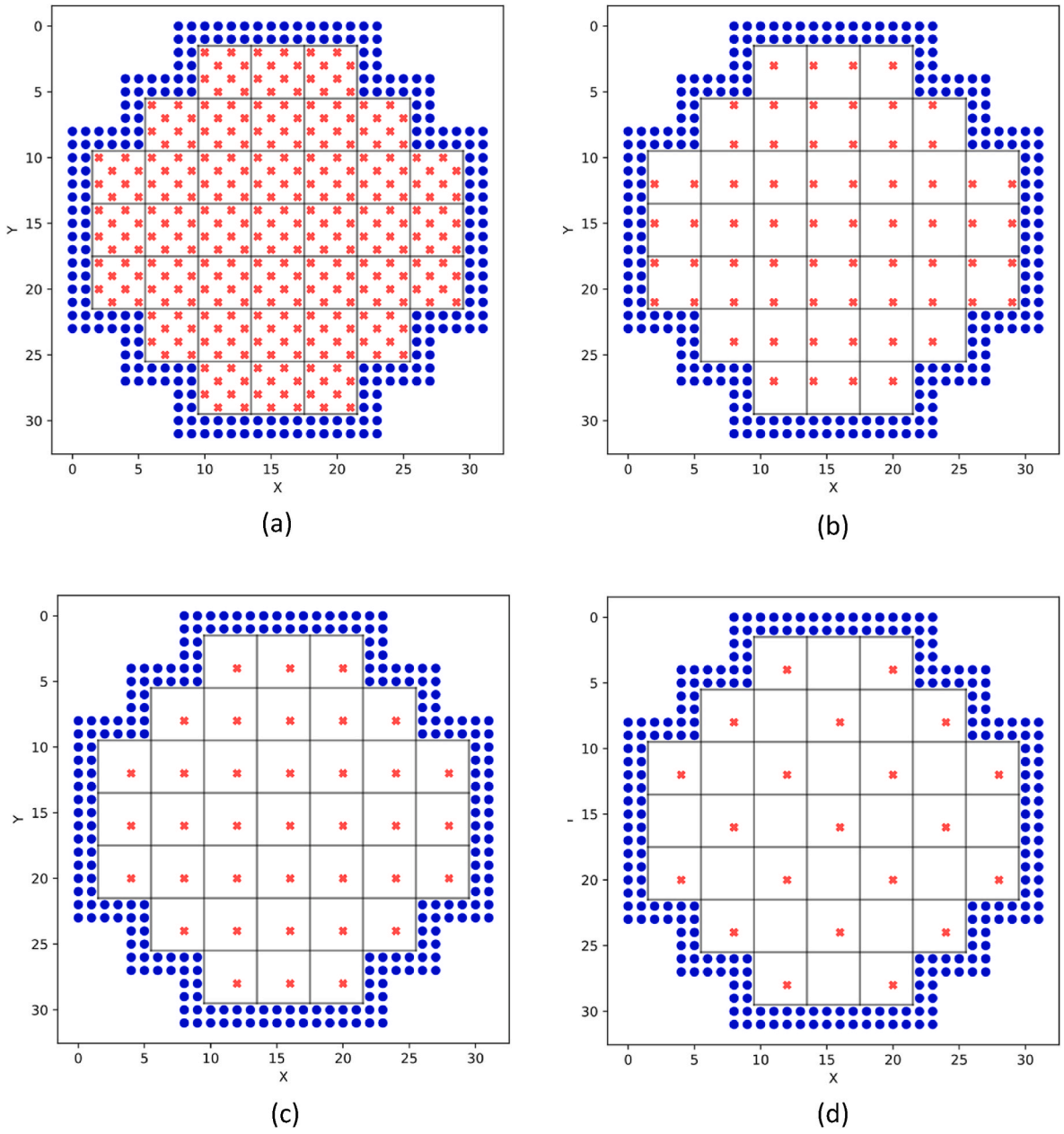

Fig. 9. Layouts for 4 cases with different instrumentation coverage densities. a. 50 %, b. 11 %, c. 6 %, and d. 3 %. The blue nodes represent the reflector, the red nodes represent the positions of detectors.

Table 3
Test MSE for reconstruction model using 50 % detector coverage.

N. of sources	1	2	3	4	5	6	7	8	9	10
MSE	3.8×10^{-5}	0.00018	0.00029	0.00043	0.00057	0.00074	0.00091	0.00108	0.00127	0.00146

performance of the pipeline. If the detected source falls within a defined range in the vicinity of the true source, it is considered correct within a margin of acceptable deviation in detection. In Fig. 11, we present the exact performance in addition to results assessed at three different proximity levels: 3×3, 5×5, and 7×7 as described in Fig. 12. For example, in the 3x3 proximity, a source detected within one node of the true source location is considered correctly detected. This means that the detected source can be one node away in any direction, forming a 3x3 area centered around the true source. The localization results of the pipeline show high precision, recall, and F1 scores for single and multiple AVS sources as shown in Fig. 11. The performance enhances as a wider proximity range is considered; however, the exact performance is still considerably very good, with recall, precision, and F1 score as high as 0.94, 0.98, and 0.06, respectively, for 10 AVS source cases. While cases involving multiple sources are generally more difficult to localize accurately, using a relaxed proximity threshold helps account for small spatial errors. In such cases, incorrect predictions often fall near one of the true source locations, which still counts as a correct detection under the proximity range. On the other hand, in single source cases, incorrect predictions are more likely to be far from the actual source. As a result,

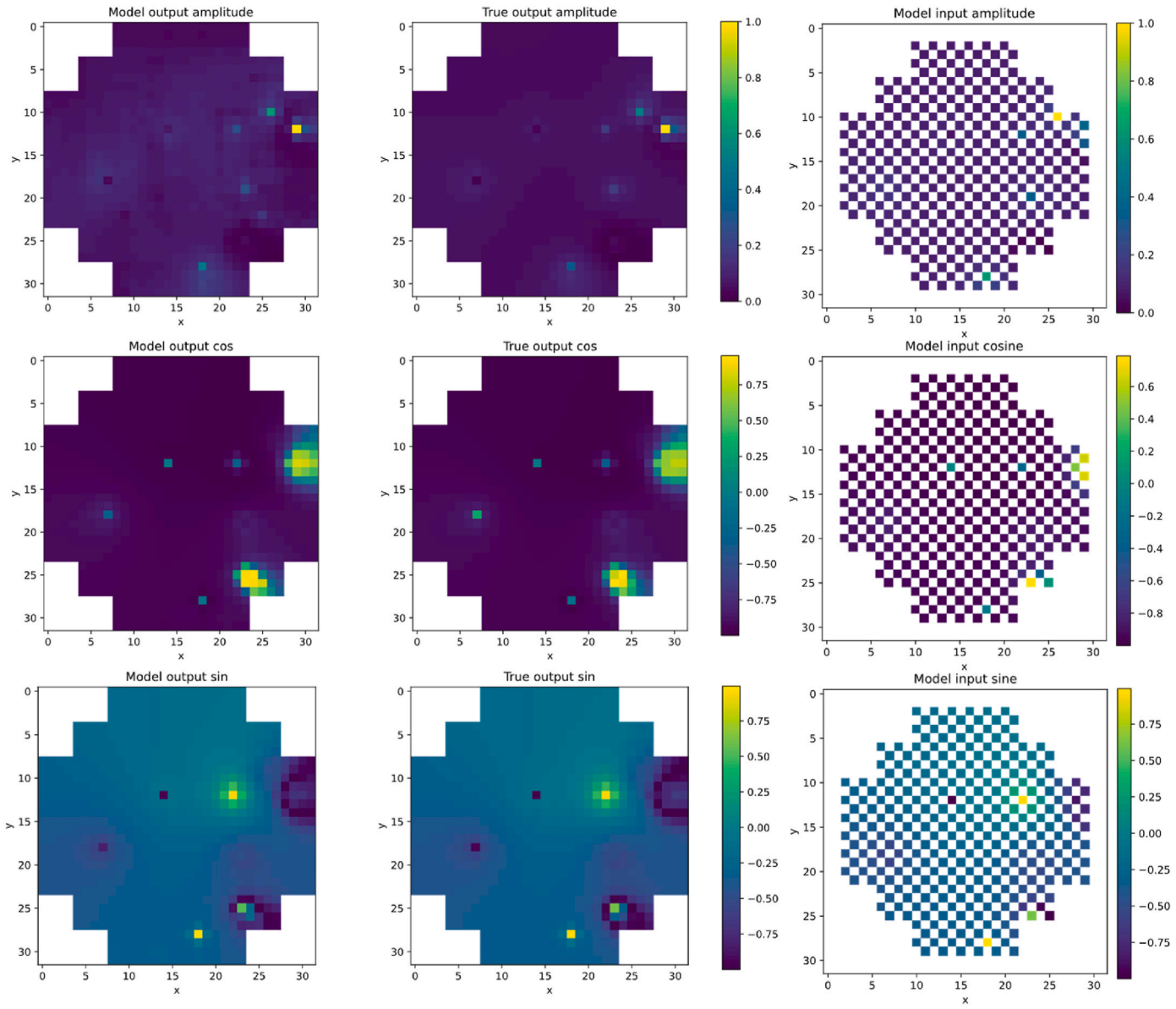

Fig. 10. Example for the reconstruction model with 8 AVS sources. The upper row shows the amplitude, the middle row shows the cosine phase, and the lower row shows the sine phase. The right column shows the input to the model with only 50 % data available in the system, the middle column is the full true induced neutron noise representation, and the left column is the induced neutron noise reconstructed by the model.

even though multi-source localization is more complex, the precision score can appear higher than in single source cases when evaluated with proximity tolerance.

It is worth mentioning that both precision and recall are important for evaluating the performance of the proposed localization model. However, in the context of reactor core monitoring, recall holds particular significance, as missing a true perturbation could lead to more serious safety implications.

The final output for the reconstruction example given in Fig. 10, is displayed in Fig. 13, showing that having 50 % less detector points does not significantly impact the AVS localization performance.

5.3.2. *Results for 11 %, 6 %, and 3 % instrumentation coverage*

To evaluate pipelines with significantly reduced instrumentation, the test cases are conducted for models with detector coverage reduced to 11 %, 6 %, and 3 % as discussed earlier. For each pipeline, the reconstruction accuracy and AVS localization performance are analyzed.

The reconstruction models are tested to assess their ability to infer the full relative neutron noise field with highly limited data. The test MSE for these cases is presented in Fig. 14, indicating a steady increase in reconstruction error as detector coverage decreases and as the number of AVS sources increases. Despite the challenges posed by reduced instrumentation, the model retains a reasonable ability to reconstruct global noise patterns.

After reconstruction, the full relative thermal noise is then used to localize AVS sources. The localization performance of the pipelines for 11 %, 6 %, and 3 % detector coverage is summarized in Figs. 15–17, respectively. The metrics include precision, recall, and F1 scores for exact detection as well as for different proximity levels as described in Fig. 12.

As expected, reducing the number of detectors leads to a progressive decrease in the exact performance, particularly as the number of AVS sources increases. For different coverage levels, precision and recall for exact localization are substantially lower compared to the 50 % coverage case. However, when using wider proximity levels, the performance improves notably, showing that the pipeline can

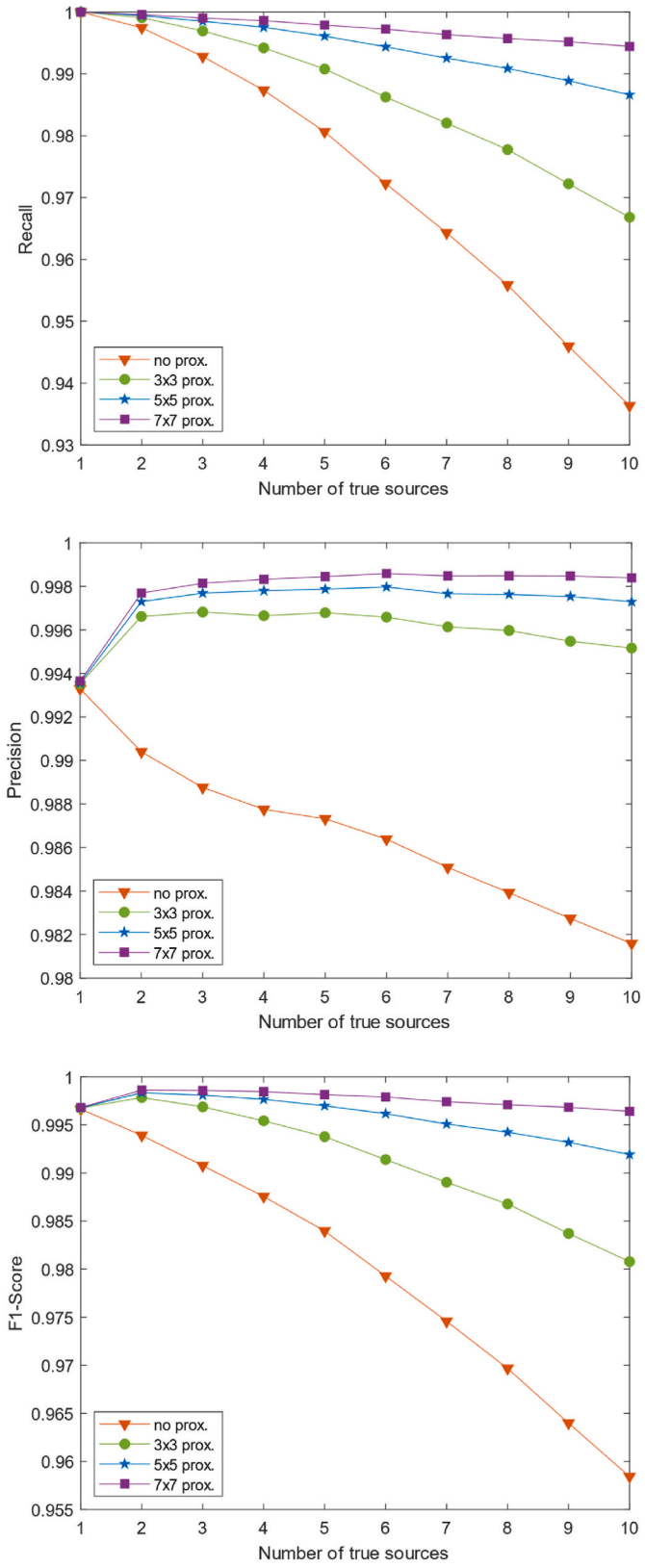

Fig. 11. Different proximity metrics for pipeline performance of 50 % detector coverage.

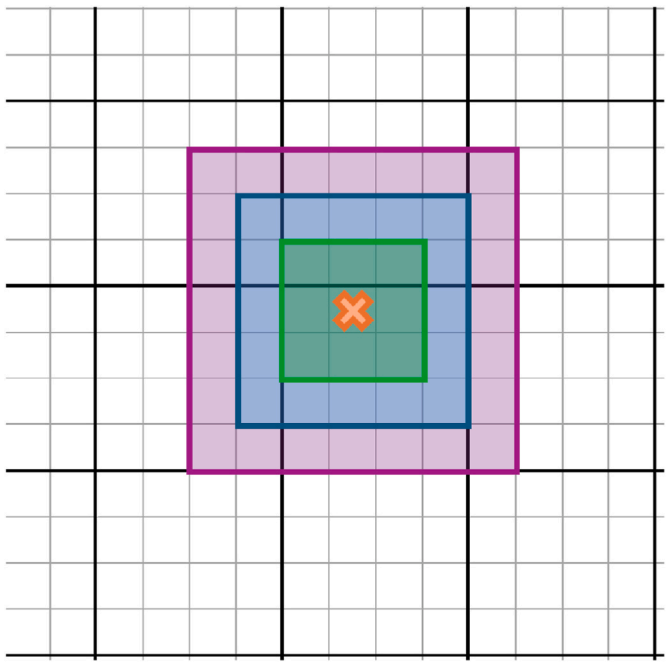

Fig. 12. Diagram showing different proximities used in assessing the performance of the pipeline. The orange: no proximity, the green: 3x3 proximity, blue: 5x5 proximity, and purple: 7x7 proximity.

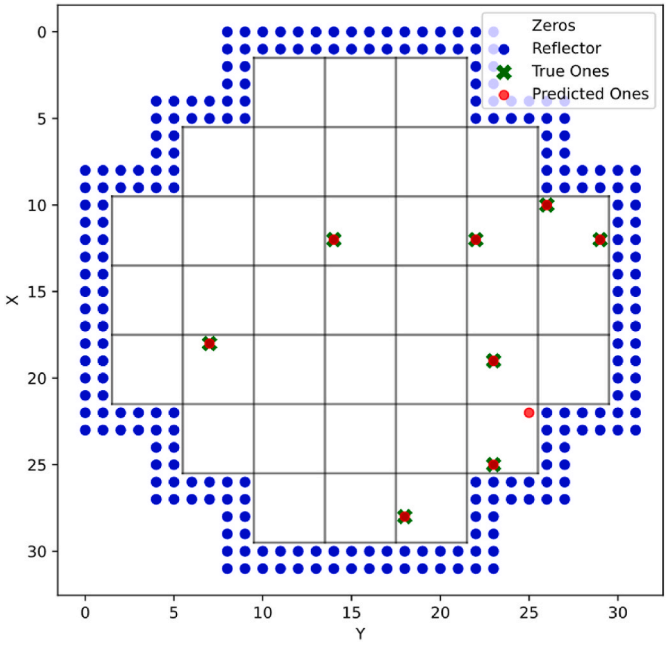

Fig. 13. Pipeline results for a 50 % detector coverage case with 8 AVS sources.

approximately identify AVS source locations even in conditions with limited instrumentation. When evaluating precision and recall across different proximities, both show significant improvement for the 11 % and 6 % coverage cases, even within a small range like 3 × 3. This suggests that in the majority of the cases the predicted sources are close to the true locations, although they may sometimes be identified as multiple adjacent sources, or with minor deviations from their true locations due to the limited detector coverage.

For sparser distribution of detectors as in the case of 3 % instrumentation coverage, the task becomes more challenging. This is demonstrated by a reconstruction example with 8 AVS sources shown in

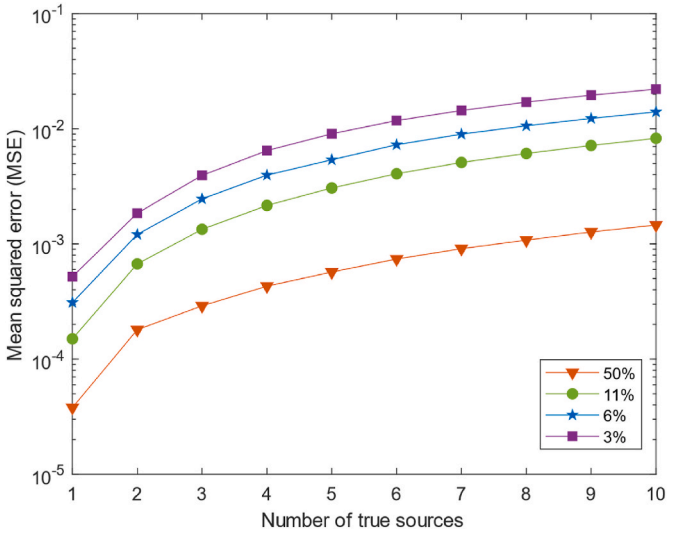

Fig. 14. Test MSE for reconstruction model using 50 %, 11 %, 6 %, and 3 % detector coverage.

Fig. 18, where the final localization output is presented in Fig. 19. The reconstructed relative thermal reactor noise closely aligns with the true reactor noise field in regions influenced by the global component, demonstrating the model's ability to capture broad noise behavior. The local noise component, which requires more spatially dense data for accurate reconstruction, is notably less pronounced in the reconstructed field. Nevertheless, the model is able to infer the approximate locations of most noise sources with reduced precision and recall compared to higher coverage cases.

The reduced instrumentation study highlights the challenges of AVS localization in systems with sparse detector coverage. At 3 % coverage, the model's reliance on the global noise component became evident, with local information largely unavailable. Despite this limitation, the pipeline still demonstrates the ability to infer approximate noise source locations, particularly when evaluated using broader proximity ranges.

6. Discussion and conclusions

In this study, a core monitoring technique for SMRs using neutron noise and ML was investigated. CORE SIM+ was used to simulate AVS-type perturbations in the frequency domain with frequency of 1 Hz. We compared the behavior of reactor noise in large and small reactors and found that the point-kinetic behavior is more dominant in smaller systems making it more challenging to diagnose perturbations in SMRs. This challenge was clearer when we analyzed the global and local components of the neutron noise and examined their deviation from point-kinetics behavior. The global component, i.e., the component responsible for observing the neutron noise at distant locations from the neutron noise source, was closely related to the point-kinetic component in small systems compared to large ones. This reactor noise nature highlighted the difficulties in detecting and localizing perturbations with limited instrumentation. Furthermore, we demonstrated the behavior of the fast-group and thermal-group neutron noise and their deviation from point-kinetics behavior showing that the thermal noise contains more useful information for the localization of noise sources.

This study demonstrated the ability of our CNN to localize up to 10 1 Hz AVS sources with very high nodal accuracy using the full relative thermal reactor noise distribution. This showed the generalization ability of the model since it was trained using samples containing 1 and 2 sources only. To account for the limitations in detectors inside a reactor core, we used a two-model pipeline where we reconstructed the reactor noise distribution from a few available points before localizing the AVS sources. The performance of the pipeline with 50 % reduced

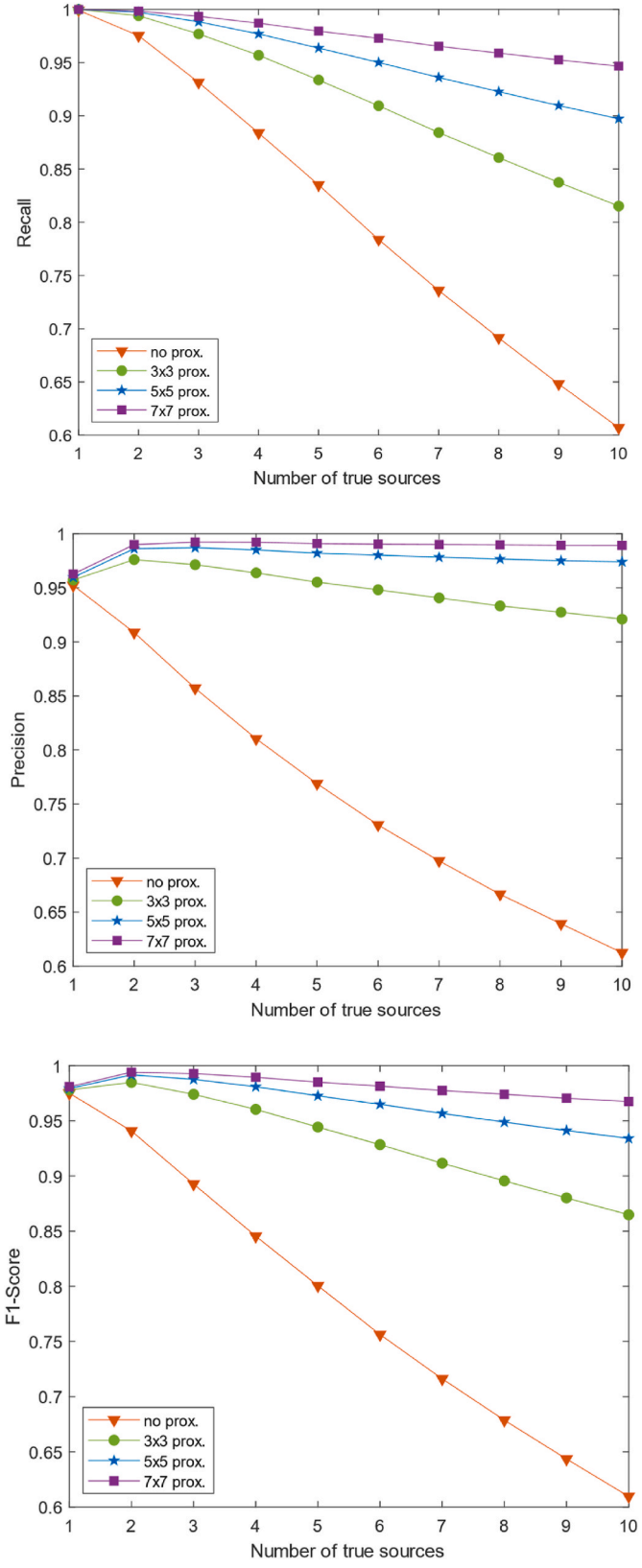

Fig. 15. Results for different proximity metrics for pipeline performance of 11 % detector coverage.

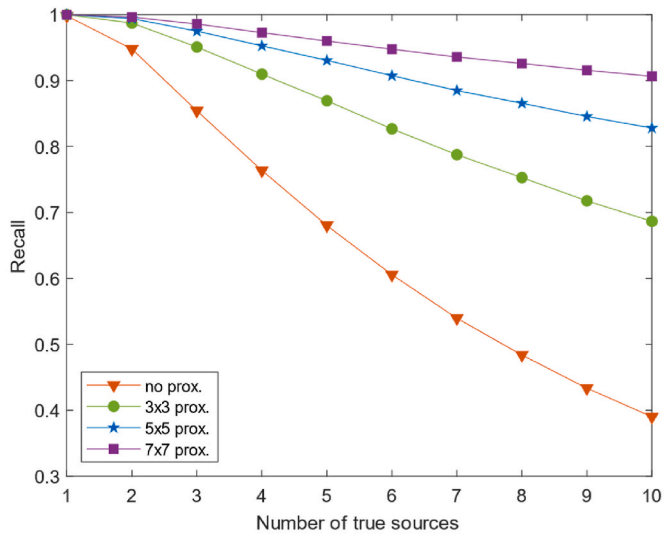

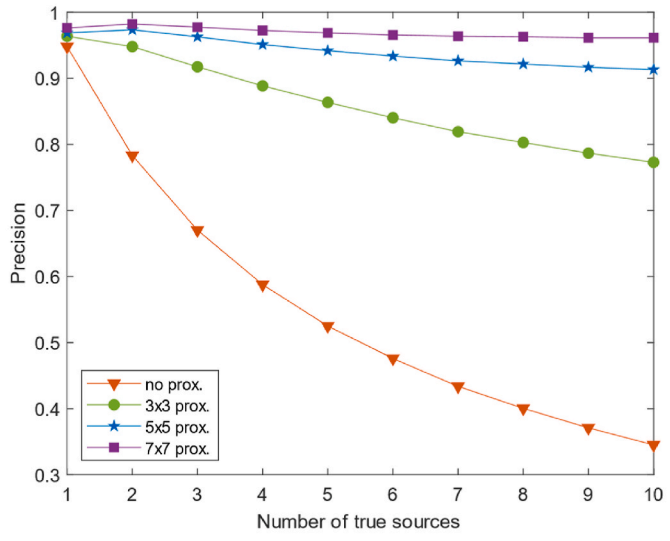

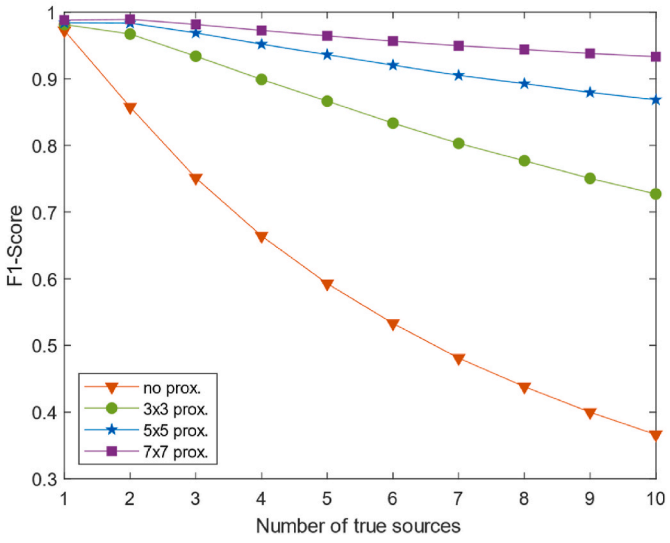

Fig. 16. Results for different proximity metrics for pipeline performance of 6 % detector coverage.

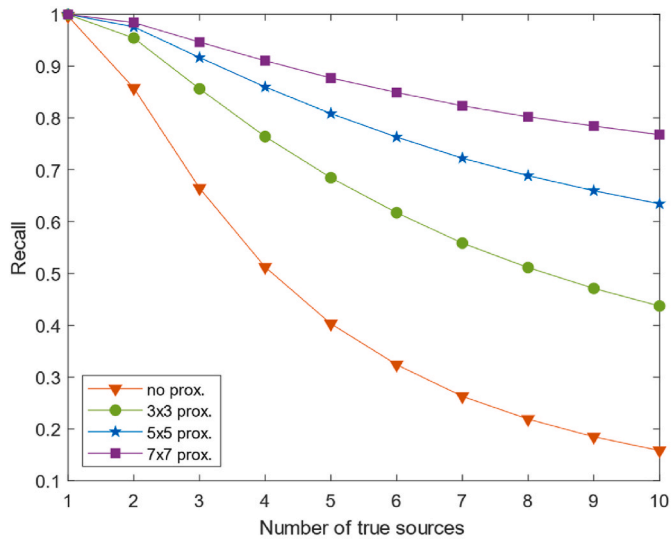

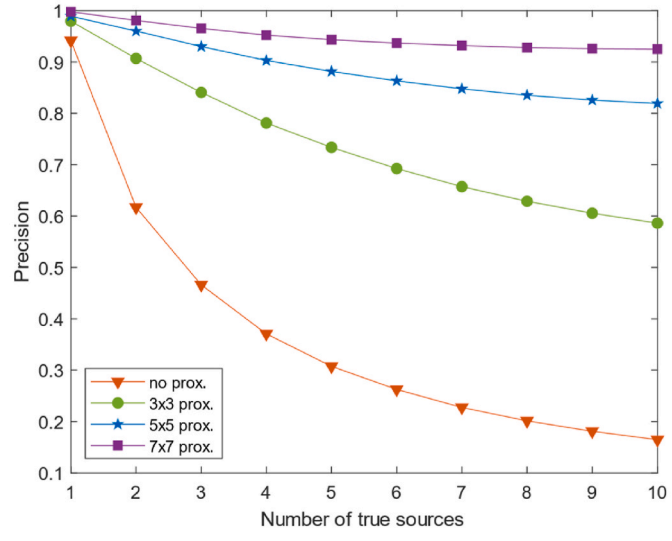

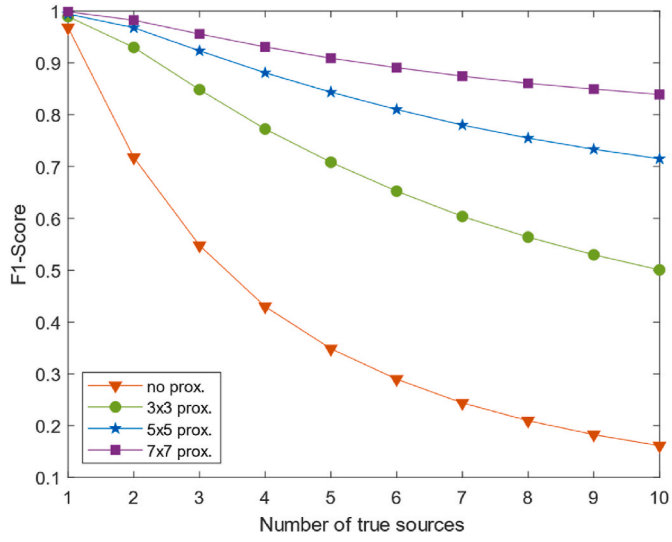

Fig. 17. Results for different proximity metrics for pipeline performance of 3 % detector coverage.

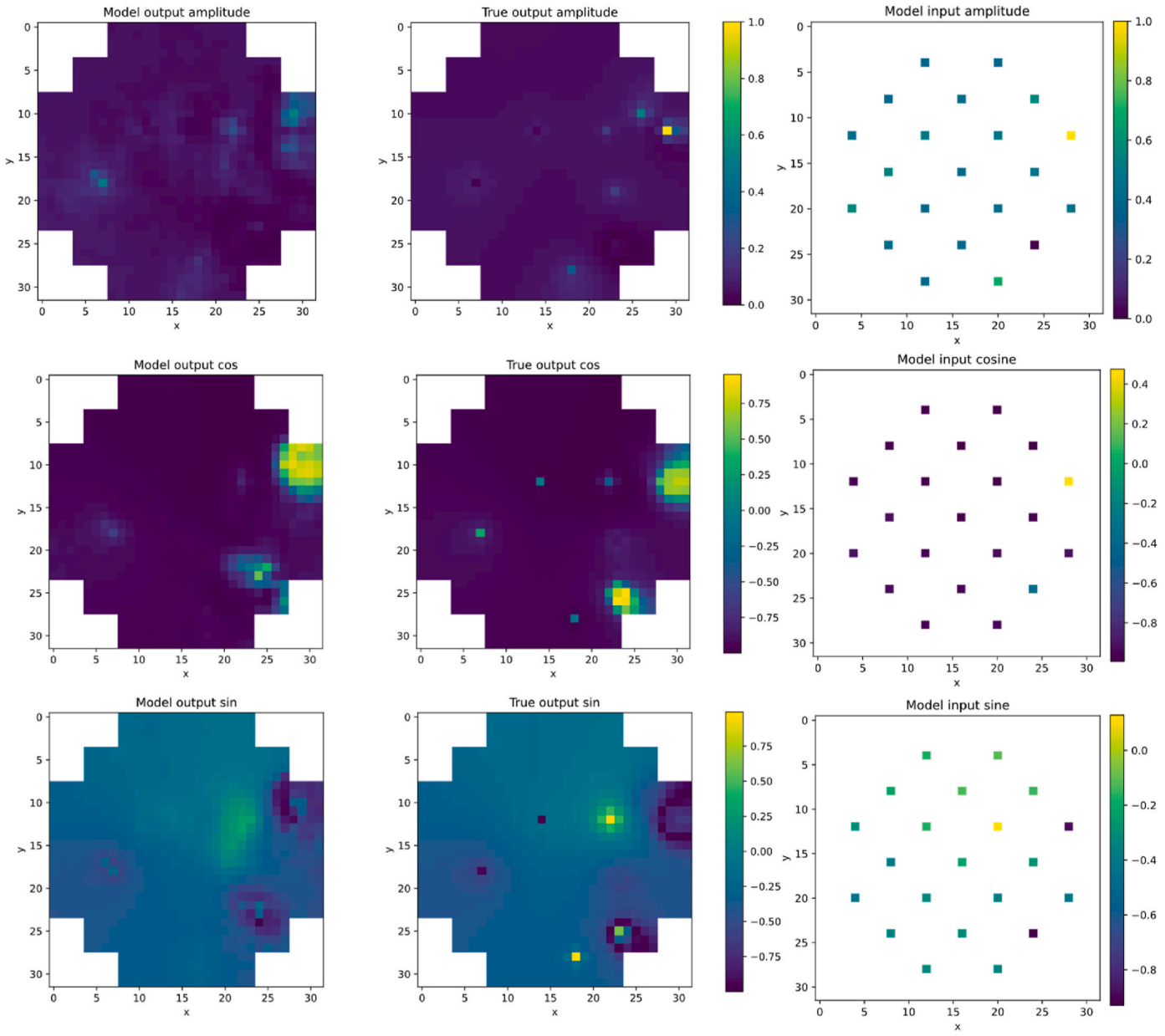

Fig. 18. Example for the reconstruction model with 8 AVS sources. The upper row shows the amplitude, the middle row shows the cosine phase, and the lower row shows the sine phase. The right column shows the input to the model with only 3 % data available in the system, the middle column is the full true noise representation, and the left column is the noise reconstructed by the model.

instrumentation shows the ability to reconstruct both the global and local components of the noise. Thus, the model was able to accurately locate the AVS sources, especially when considering AVS predicted within the vicinity of the true source as correctly predicted.

More practical cases were considered with a significant decrease in instrumentation, i.e., with 11 %, 6 %, and 3 % detector coverage. In these cases, the performance of the pipeline gradually decreased, but the model still demonstrated a reasonable ability to infer the approximate locations of AVS sources, especially when evaluated with wider proximity metrics. These results highlighted the importance of both the global and local noise components, as the model tended to rely on global noise information when detector coverage was sparse.

The results displayed the challenges posed by limited instrumentation in SMRs where sensor placement is often sparse and limited. However, the ability of the pipeline to effectively localize AVS sources with reduced data suggested that further advancements in reconstruction algorithms could improve the performance under limited conditions. Future research should focus on enhancing the accuracy of source localization in low-density detector systems and exploring how prior knowledge of reactor behavior can be integrated into these models to further improve performance in realistic operational environments.

This research provided a foundation for advancing monitoring techniques in SMRs and highlights the potential of ML-based methods to improve safety and reliability in next-generation reactor designs. Even though the localization model was trained on simulated data, the results remain relevant, since nuclear reactor applications in real-life will need to rely on simulated data for training ML models. The findings highlighted the importance of strategically positioning detectors to maximize coverage of both global and local noise components. It also emphasized the need for careful instrumentation planning in the design phase of SMRs to ensure effective noise source localization, even with sparse detector networks.

Future work will expand this study by transitioning from the current two-dimensional analysis to realistic three-dimensional models of SMRs.

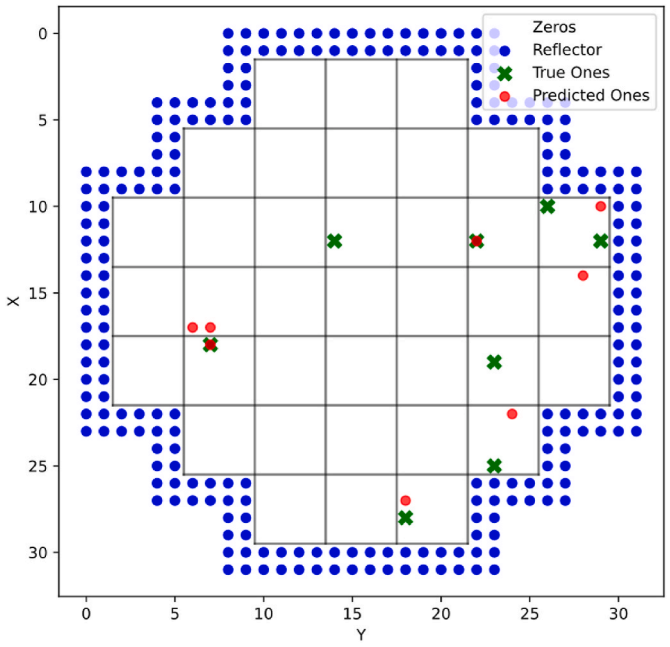

Fig. 19. Pipeline results for a 3 % detector coverage case with 8 AVS sources.

This will enable a more comprehensive understanding of neutron noise behavior in small systems including vertical spatial variations. Additionally, future investigations will incorporate a broader range of perturbation types, such as coolant flow perturbations and fuel assembly vibrations, thereby addressing more complex and realistic reactor scenarios. These perturbations will be analyzed across a wider spectrum of frequencies. In addition, uncertainty quantification will be applied at different stages of the methodology, to evaluate the robustness of the proposed ML model under non-ideal and more realistic conditions. Furthermore, a comprehensive ML framework that identifies and localizes different perturbations with no prior reconstruction requirements will be explored. The insights gained will help improve the design of SMR instrumentation, leading to safer and more efficient next-generation nuclear reactors. Furthermore.

CRediT authorship contribution statement

Salma Magdi Hussein: Writing – original draft, Visualization, Validation, Software, Methodology, Investigation, Formal analysis, Data curation, Conceptualization. **Christophe Demazière:** Writing – review & editing, Supervision, Project administration, Methodology, Investigation, Funding acquisition, Formal analysis, Conceptualization.

Declaration of generative AI and AI-assisted technologies in the writing process

During the preparation of this work, the authors used ChatGPT in order to improve the grammar and language tone. After using this tool, the authors reviewed and edited the content as needed and take full responsibility for the content of the published article.

Declaration of competing interest

The authors declare that they have no known competing financial interests or personal relationships that could have appeared to influence the work reported in this paper.

Acknowledgments

This research has been conducted within ANItA – Academic-industrial Nuclear technology Initiative to Achieve a sustainable energy future, which is financed by Swedish academia, the Swedish nuclear industry and the Swedish Energy Agency.

The data generated by CORESIM+ and the ML computations were enabled by resources provided by the National Academic Infrastructure for Supercomputing in Sweden (NAISS), partially funded by the Swedish Research Council through grant agreement no. 2022–06725.

Associate Professor Paolo Vinai is acknowledged for joint discussions on some aspects of the project.

Data availability

The authors are unable or have chosen not to specify which data has been used.

References

Agarwal, K., Toshniwal, D., Gupta, P.K., Khurana, V., Upadhyay, P., 2013. Anomaly detection and similarity search in neutron monitor data for predictive maintenance of nuclear power plants. Proceedings - 2nd International Conference on Advanced Computing, Networking and Security, ADCONS 2013. Mangalore, India.

Analytis, G.T., 1979. A three-dimensional theoretical investigation of the local and global component of the neutron noise in bare homogenous water moderated reactors and applications. Ann. Nucl. Energy 7 (6), 351–366.

De Hoffman, F., 1946. Intensity Fluctuations of a Neutron Chain Reactor, vol. 382. U.S. Atomic Energy Commission. https://catalog.hathitrust.org/Record/007841354.

Demazière, C., 2025. Editorial. Ann. Nucl. Energy 212, 110938. https://doi.org/10.1016/j.anucene.2024.110938.

Demazière, C., Andhill, G., 2005. Identification and localization of absorbers of variable strength in nuclear reactors. Ann. Nucl. Energy 32 (8), 812–842. https://doi.org/10.1016/j.anucene.2004.12.011.

Demazière, C., Rouchon, A., Zoia, A., 2022. Understanding the neutron noise induced by fuel assembly vibrations in linear theory. Ann. Nucl. Energy 175 (109169). https://doi.org/10.1016/j.anucene.2022.109169.

Dubey, S.R., Singh, S.K., Chaudhuri, B.B., 2022. Activation functions in deep learning: a comprehensive survey and benchmark. Neurocomputing 503, 92–108. https://doi.org/10.1016/j.neucom.2022.06.111.

Durrant, A., Leontidis, G., Kollias, S., 2019. 3D convolutional and recurrent neural networks for reactor perturbation unfolding and anomaly detection. EPJ Nucl. Sci. Technol. 5 (20). https://doi.org/10.1051/epjn/2019047, 2019.

Hosseini, S.A., Vosoughi, N., 2014. Noise source reconstruction using ANN and hybrid methods in VVER-1000 reactor core. Prog. Nucl. Energy 71, 232–247. https://doi.org/10.1016/j.pnucene.2013.12.007.

Hursin, M., Zoia, A., Rouchon, A., Brighenti, A., Zmijarevic, I., Santandrea, S., Vinai, P., Mylonakis, A., Yi, H., Demazière, C., Lamirand, V., Ambrozic, K., Yamamoto, T., Hübner, S., Knospe, A., Lange, C., Yum, S., Macian, R., Vidal, A., Verdú, G., 2023. Modeling noise experiments performed at AKR-2 and CROCUS zero-power reactors. Ann. Nucl. Energy 194, 110066. https://doi.org/10.1016/j.anucene.2023.110066.

Hussein, E.M.A., 2020. Emerging small modular nuclear power reactors: a critical review. Phys. Open 5 (100038). https://doi.org/10.1016/j.physo.2020.100038.

Hussein, S.M., Vinai, P., Demazière, C., 2024. On reactor neutron noise induced by fuel assembly vibrations in large and small heterogenous water-cooled cores. International Conference on Physics of Reactors (PHYSOR 2024). San Fransisco, USA.

IAEA, 2013. Advanced Surveillance, Diagnostic and Prognostic Techniques in Monitoring Structures, Systems and Components in Nuclear Power Plants. IAEA, Vienna. No. NP-T-3.14. https://www.iaea.org/publications/8763/advanced-surveillance-diagnostic-and-prognostic-techniques-in-monitoring-structures-systems-and-components-in-nuclear-power-plants.

IAEA, 2022a. Advances in Small Modular Reactor Technology Developments A Supplement To: IAEA Advanced Reactors Information System (ARIS). IAEA, Vienna. https://aris.iaea.org/Publications/SMR_Book_2020.pdf.

IAEA, 2022b. Artificial Intelligence for Accelerating Nuclear Applications, Science and Technology. IAEA, Vienna. https://www.iaea.org/publications/15198/artificial-intelligence-for-accelerating-nuclear-applications-science-and-technology.

Kamkar, A., Abbasi, M., 2025. A comparative study of machine learning approaches for identification of perturbed fuel assemblies in WWER-type nuclear reactors. Ann. Nucl. Energy 211, 110992. https://doi.org/10.1016/j.anucene.2024.110992.

Kingma, D.P., Ba, J., 2015. *Adam: a Method for Stochastic Optimization* International Conference on Learning Representations (ICLR) 2015. San Diego, CA, USA.

Kollias, S., Yu, M., Wingate, J., Durrant, A., Leontidis, G., Alexandridis, G., Stafylopatis, A., Mylonakis, A., Vinai, P., Demaziere, C., 2022. Machine learning for analysis of real nuclear plant data in the frequency domain. Ann. Nucl. Energy 177, 109293. https://doi.org/10.1016/j.anucene.2022.109293.

LeCun, Y., Bengio, Y., Hinton, G., 2015. Deep learning. Nature 521, 436–444. https://doi.org/10.1038/nature14539.

Moore, M.N., 1958. The determination of reactor transfer functions from measurements at steady operation. Nucl. Sci. Eng. 3 (4), 387–394. https://doi.org/10.13182/NSE58-A25476.

Mylonakis, A., Vinai, P., Demazière, C., 2021. Core SIM+: a flexible diffusion-based solver for neutron noise simulations. Ann. Nucl. Energy 155, 108149. https://doi.org/10.1016/j.anucene.2021.108149.

Pázsit, I., Demazière, C., 2010. Noise Techniques in Nuclear Systems. Springer. https://doi.org/10.1007/978-0-387-98149-9_14.

Rajagopal, V., 1962. Determination of reactor transfer functions by statistical correlation methods. Nucl. Sci. Eng. 12 (2), 218–224. https://doi.org/10.13182/NSE62-A26060.

Ronneberger, O., Fischer, P., Brox, T., 2015. U-Net: Convolutional networks for biomedical image segmentation. Med. Image Comput. Comput. Assist. Interv. MICCAI 2015 9351, 234–241. https://doi.org/10.1007/978-3-319-24574-4_28.

Szegedy, C., Vanhoucke, V., Ioffe, S., Shlens, J., Wojna, Z., 2016. *Rethinking the inception architecture for computer vision* 2016. In: IEEE Conference on Computer Vision and Pattern Recognition (CVPR). https://doi.org/10.1109/CVPR.2016.308 ieeecomputersociety.org.

Terven, J.R., Córdova-Esparza, D.-M., Ramírez-Pedraza, A., Chavez-Urbiola, E.A., Romero-González, J.-A., 2023. A comprehensive survey of loss functions and metrics in deep learning. Artif. Intell. Rev. 58. https://doi.org/10.1007/s10462-025-11198-7.

Thie, J.A., 1963. Reactor Noise. Rowman and Littlefield. https://catalog.hathitrust.org/Record/001627895.

Thie, J.A., 1981. Power Reactor Noise. American Nuclear Society.

Weinberg, A.M., Schweinler, H.C., 1948. Theory of oscillating absorber in a chain reactor. Phys. Rev. 74 (8), 851–863. https://doi.org/10.1103/PhysRev.74.851.

Williams, M.H.P., 1974. Random Processes in Nuclear Reactors. Pergamon Press. https://doi.org/10.1109/TNS.1975.4328076.